Large-Acceptance Multi-Particle Spectrometer

SAMURAI

(**S**uperconducting **A**nalyzer for **Mu**lti-particle from **Ra**dio **I**sotope Beams)

Construction Proposal

Abstract

We proposed and started to construct a large-acceptance multi-particle spectrometer SAMURAI for radioactive-beam experiments. The central part of the spectrometer system is a large-gap superconducting magnet with 7 Tm of bending power for momentum analysis of heavy projectile fragments and projectile-rapidity protons with large angular and momentum acceptance. The large gap also enables measurements of projectile-rapidity neutrons with large angular acceptance in coincidence with heavy projectile-like fragments.

This system is suitable for various radioactive-beam experiments such as electromagnetic dissociation including radiative-capture reactions, various direct reactions as well as polarized-deuteron-induced reactions and EOS studies.

The major construction was started by a four-year budget approved in 2008. Construction of experimental devices which are covered by this budget is completed in 2011, and the operation for radioactive-beam experiments is planned to start in early 2012. This proposal provides outline and current status of the project including magnet and detector construction, and also an overview of the plan of experiments to perform in early stage of the operation.

Members of Collaboration

Spokesperson	T. Kobayashi (Tohoku Univ.)
Co-Spokesperson	T. Motobayashi (RIKEN)
Project Manager	K. Yoneda (RIKEN)

Construction Team	Member (*Leader of the Team)
Magnet and Infrastructure:	H. Sato[*], K. Kusaka, J. Ohnishi, H. Okuno, T. Kubo (RIKEN)
Vacuum system and Utilities:	H. Otsu[*], Y. Shimizu (RIKEN)
Heavy ion detectors:	Y. Matsuda, K. Sekiguchi, N. Chiga, graduate students, T. Kobayashi* (Tohoku), H. Otsu (RIKEN)
Neutron detectors (NEBULA):	T. Nakamura*, Y. Kondo, Y. Kawada, T. Sako, R. Tanaka (Tokyo Tech), Y. Satou (Seoul National Univ.)
Proton detectors:	K. Yoneda*, Y. Togano, M. Kurokawa, A. Taketani, H. Murakami, T. Motobayashi (RIKEN), K. Kurita (Rikkyo), T. Kobayashi (Tohoku), L. Trache (Texas A&M) and the TWL collaboration
Polarized deuteron induced reaction experiment devices:	
	K. Sekiguchi*, T. Kobayashi, Y. Matsuda, graduate students (Tohoku)
Time projection chamber:	T. Murakami* (Kyoto), T. Isobe, A. Taketani, S. Nishimura, Y. Nakai, H. Sakurai (RIKEN), W.G. Lynch (Michigan State) and SAMURAI TPC collaboration

In-House Work Force: Research Instruments Group (T. Kubo - Group Leader)

SAMURAI Team (T. Motobayashi*, H. Sato, Y. Shimizu, K. Yoneda)

Table of Contents

[1] Overview

[1-1] Introduction

This construction proposal contains description of SAMURAI (**S**uperconducting **A**nalyzer for **Mu**lti-particle from **R**adio **I**sotope Beams), status and plan of its construction and experimental programs we wish to perform in an early stage of its operation.

The idea to construct a spectrometer with large angular- and momentum-acceptance as equipment in the RI Beam Factory (RIBF) has been discussed for long time. Its design was presented and evaluated in the Technical Advisory Committee (TAC) Meeting held in November 2005. Encouraged by the statement "…the Samurai spectrometer is an essential part of the exotic nuclei research where different types of reactions are employed…" in the TAC report, we continued design works and started construction in the fiscal year 2008, when a four-year budget for SAMURAI construction was approved.

This proposal was made by the SAMURAI Collaboration with members involved in the construction works at present. In order to have more involvement of scientists in the world for developing research with SAMURAI, the SAMURAI collaboration should be extended to more researchers who are interested in SAMURAI-based experiments. An international workshop is planned in early 2011 to discuss possible research programs in collaboration.

The SAMURAI spectrometer has been designed to optimize the coincidence measurement between heavy projectile fragments and projectile-rapidity neutrons/protons with large angular and momentum acceptance. A schematic view of SAMURAI is shown in Fig. 1-1-1. SAMURAI consists of a wide-gap high-field superconducting magnet and various particle detectors for experiments using RI beams from BigRIPS at RIBF. This design allows measurements of reactions with unbound final states and hence studies on the properties of the unbound excited states as well as those of the ground state of nuclei away from the stability valley on both the neutron- and proton-rich sides.
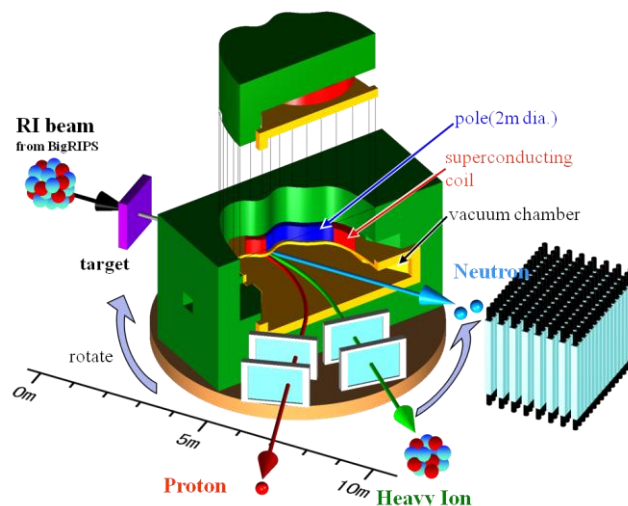

Fig 1-1-1: Schematic view of SAMURAI spectrometer

The regions in the nuclear chart and the asymmetry-energy plane where the studies with SAMURAI are planned are indicated in Figs. 1-1-2 and 1-1-3, respectively. Coupled with the high RIBF capability, SAMURAI may have access to the following unexplored regions indicated in the figures. The first focus will be on the neutron- and proton-rich regions with mass number A lower than approximately 100, where reasonable particle (isotope) identification could be performed because ions in that region are mostly fully stripped. There expect various interesting physics in exotic properties of neutron drip-line nuclei, such as neutron halo, neutron correlations, unbound states beyond the drip line, and new cluster/molecular states as indicated in Fig. 1-1-2. These phenomena should be observed in unbound final states of reactions near the drip line as seen in Fig. 1-1-3, and well suited for measurements with SAMURAI. On the proton-rich side, astrophysical processes involved in explosive hydrogen burning, *e.g.* the rp process, are governed by the properties of proton-rich nuclei in the region just above the proton threshold (see also in Fig. 1-1-3), which again is to be accessed by SAMURAI. It should be emphasized that many interesting phenomena in nuclei near the drip-lines are expected in the unbound regions of nuclear excitation. Such physics cases are in the reach of SAMRURAI.

As indicated in the figures, SAMURAI allows for approaching more cases of interest: properties of asymmetric nuclear matter studied by "pigmy" giant resonances, the nuclear equation of state studied by multi-fragmentation process, studies on neutron skins by, for example, elastic scattering measurements and so on. Specific r-process neutron captures can also be investigated by the properties of neutron unbound-states in nuclei around the neutron magic numbers. Three-nucleon forces can also be studied in the interaction between polarized deuteron and proton. The large acceptance of SAMURAI enables efficient and precise measurement of cross sections and spin-dependent observables.
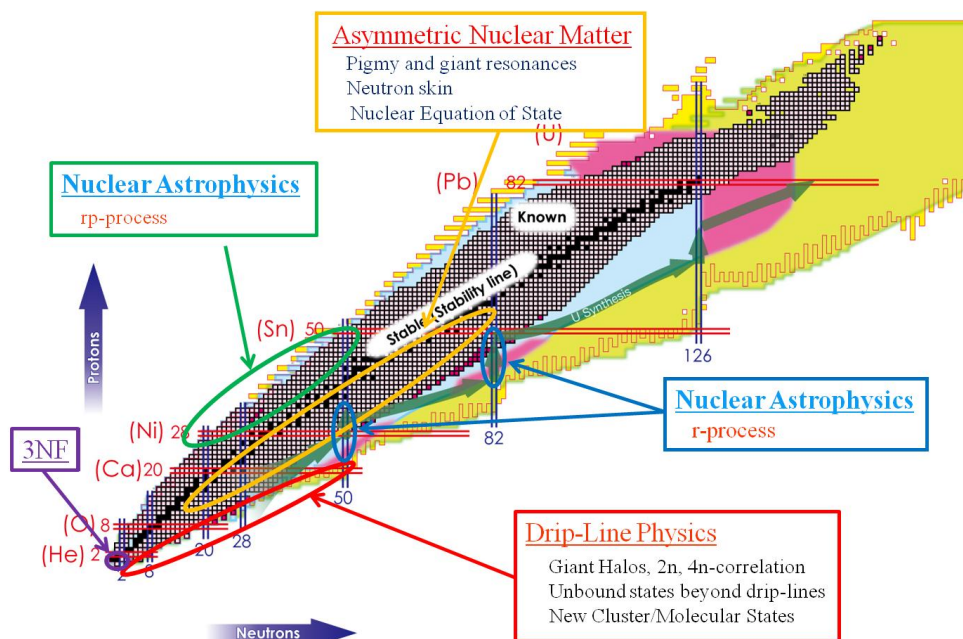

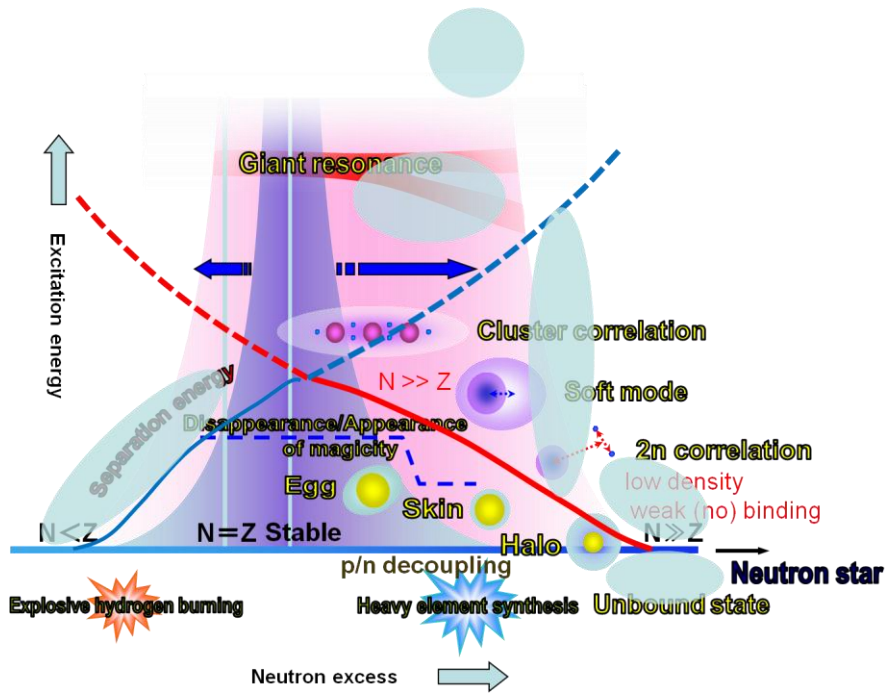Fig 1-1-2: Mass region of interest in nuclear chart

Fig 1-1-3: Region of interest in asymmetry vs excitation energy plain

The (γ,n)-type experiment is one of the n-HI coincidence experiments by utilizing the Coulomb excitation. These experiments focus on the physics of neutron drip-line, asymmetric nuclear matter, and nuclear astrophysics. The reaction is used to study

* exotic ground-state properties such as the neutron halo in the drip-line nuclei,
* unbound ground state properties of nuclei beyond the drip line,
* pigmy and giant resonances in nuclei with large neutron-proton asymmetry
* nuclei in the r process.

Combination of high intensity beams available at RIBF and SAMURAI spectrometer provides a good access to various neutron-rich nuclei which cannot be reached so far.

The HI-p coincidence enables a series of Coulomb dissociation experiments of astrophysical interest: (p,γ) reaction in the rp process and (γ,p) reaction in the p-process. Situation is the same on the proton-rich side: various proton-rich nuclei which cannot be reached can be accessed.

Considering the uniqueness of SAMURAI at RIBF, the first experiments are planned as summarized in Table 1-1-1.

reaction type	starting period	first experiments
(γ,n)-type	early 2012	1n-halo (^{31}Ne)…
	early 2012	unbound g.s. (^{26}O) …
	mid 2012	pigmy resonance ($^{72-76}$Ni) …
(γ,p)-type	early 2013	rp waiting point (^{56}Ni, ^{64}Ge) …

Table 1-1-1: Planned first experiments

Other types of experiments exploiting the SAMURAI capability are also listed as follows.

＊ Proton elestic scattering for studying the density distributions in asymmetric nuclei

＊ Nucleon knockout reactions such as (p,2p) and (p,pn) for studying the single-particle orbits in asymmetric nuclei

＊ Polarized deuteron-induced reactions for studying the three nucleon force (3NF)

＊ Study of equation of states (EOS) in asymmetric system using TPC.

[1-2] Physics Cases

The large-acceptance multi-particle spectrometer is primarily designed for kinematically complete measurements by detecting multiple particles in coincidence, such as the invariant-mass measurement. The large bending power and large gap also enable various types of measurements. The following table summarizes the physics subjects in terms of the reaction types.

Reaction types	Category	Physics subjects	Observables
Electromagnetic dissociation (photon target)	Soft dipole excitation Giant resonance Radiative capture reaction	Single-particle orbit Collective motion Nuclear astrophysics	Invariant mass
Proton and light target	Elastic/inelastic, (p,p), (p,p') Knockout, (p,pN)	Density distribution Single-particle orbit	Missing energy & decay tagging
Polarized d beam Induced reaction	(d,d) (d,p)	2-3 nucleon force Short range correlation	polarization
4π measurement		Equation Of State	pions

(1) Soft Dipole Excitation via Coulomb Dissociation

Electromagnetic excitation by low-energy virtual photons induces direct non-resonant type excitations to continuum for neutron-rich nuclei with loosely-bound neutrons. The low-energy E1 strength can be studied utilizing invariant-mass spectroscopy by measuring the four-momenta of the outgoing heavy fragment and few neutrons in coincidence, as schematically shown in Fig.1-2-1. Such strength provides useful information on the ground state properties such as characteristics of the single-particle orbit. Measurements performed for 1-n halo nuclei ^{11}Be and ^{19}C give valuable information on the extended s-wave component of the single-particle state in light-mass region. In the new facility, measurements can be extended to N=21 and N=51 nuclei, where the lowering of 2p and 3s states are expected. In addition to the nuclear structure problems, it might be possible to extract information on the 2n correlations for neutron-rich nuclei with two weakly-bound neutrons.

Electromagnetic excitation also provides an experimental tool to observe soft dipole resonance (SDR) related to the thick neutron skin with collective nature. Although this type of resonance has never been observed in the light-mass region, measurements extended into the heavier-mass region might give

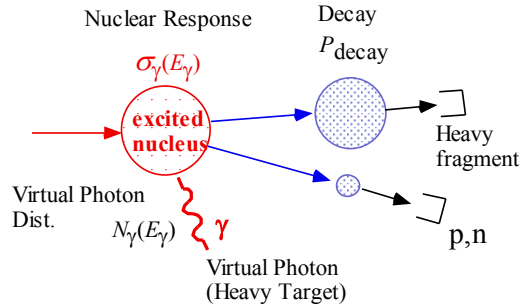information on the collective motion in a very asymmetric system.

Fig. 1-2-1: Electromagnetic dissociation via invariant-mass method

(2) Radiative Capture Cross Sections via Coulomb Dissociation

Radiative capture cross sections, $\sigma(p,\gamma)$, at low energies are of crucial importance for studying nuclear astrophysics. Electromagnetic excitation of proton-rich nuclei can be used to measure these cross sections utilizing the invariant-mass method and the principle of detailed balance.

Several reactions for the p-p chain and CNO cycle have been studied using the Coulomb dissociation method, for example, the ^{13}N(p,γ)^{14}O reaction which is a key reaction of hot-CNO cycle; ^{7}Be(p,γ)^{8}B reaction related to the solar neutrino problem; ^{22}Mg(p,γ)^{23}Al reaction relevant to break out of the NeNa cycle; ^{8}B(p,γ)^{9}C, ^{11}C(p,γ)^{12}N and ^{12}N(p,γ)^{13}O reactions relevant to hot p-p chain. Using the Big-RIPS and a large-acceptance spectrometer, the cross sections for radiative capture reactions for explosive nucleosynthesis (the rp-, r-, and s- processes) in nova, supernova, X-ray bursts, etc., are expected to be measured. From these measured cross sections, more-reliable network-calculations on the nucleosynthesis can be expected.

Coulomb dissociation of proton-rich nuclei also provides an experimental tool to study their nuclear structure, such as the occurrence of new magic numbers, near the proton drip line by observing the excited states.

(3) Direct nuclear reactions on a proton target

Direct reactions on the proton target, such as the proton elastic and inelastic scattering, (p,p) and (p,p'), and nucleon knockout reactions, (p,2p) and (p,pn), provide information on the nuclear density distribution of the whole system, spatial distribution of bound nucleons via momentum-distribution measurement, and single-particle orbit. Although the main part of these measurements is missing-energy measurement by detecting recoil nucleon(s), tagging the projectile fragment by the spectrometer allows studying the decay mode of the residual nuclei at the same time (Fig. 1-2-2).
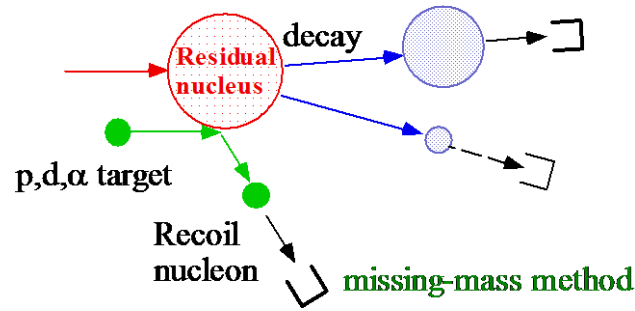
Fig. 1-2-2: Tagging the decay mode of the residual nucleus after the direct reaction

(4) Two- and Three-nucleon interactions

One of the primary goals of nuclear many-body physics is to understand nuclear structure starting from the fundamental nucleon-nucleon (NN) interactions. The state-of-the-art NN interaction models, such as CD-Bonn, Nijmegen-I, AV18, can reproduce deuteron static properties and several thousands of NN scattering data almost perfectly. Nevertheless, when the interactions are applied to nuclear structure calculations, it is revealed that the interactions alone cannot give the correct values of binding energies. Apparently, it is necessary to refine our understanding of the NN interactions to achieve the primary goal.

The purpose of this project is to improve our understandings of the nuclear interaction through polarization measurements with a primary beam of polarized deuterons with an energy of $E_d < 880$ MeV. The proposed investigations are:

- Three nucleon force effects in d+p scatterings, putting special focus on spin-dependences and relativistic effects.
- Short-range part of the NN tensor interactions probed by the polarization correlation measurements for the ^{3}He(d,p)^{4}He reaction.

(5) Asymmetry Energy of Nuclear Matter

RI beams provide a great opportunity to explore experimental constraints on the density dependence of the asymmetry energy of the nuclear equation of state (EOS). Although symmetry energy of the EOS has been well investigated through compressional giant resonances and collective flows observed in heavy ion collisions at intermediate and relativistic energies, the knowledge of asymmetric energy is still very limited.

Suggested by the recent theoretical calculations, we propose to measure the isospin dependence of π^+ and π^- production using a time projection chamber (TPC) installed in the large magnet gap for information on the density dependence of the asymmetry term at above normal densities.

[1-3] Requirements to the Detector System

Mass Region

Measurements will be performed using RI beams up to A = 100, mainly limited by the availability of fully-stripped beams, and in the energy region between 250 – 300 MeV/A. This limitation comes mainly

from the lack of the redundancy on the particle identification (PID) in the large acceptance spectrometer.

Particle identification

It is essential to identify mass and charge of the projectile fragment produced in the reaction. PID requires three independent measurements, such as charge (z), momentum (magnetic rigidity R), and velocity (β), or z, R, and total energy E. If 5 sigma mass separation ($\sigma_A = 0.2$) is required for

$A = 100$, error propagation, $\dfrac{\sigma_A}{A} = \sqrt{\left(\dfrac{\sigma_R}{R}\right)^2 + \left(\dfrac{\sigma_z}{z}\right)^2 + \left(\gamma^2 \dfrac{\sigma_\beta}{\beta}\right)^2}$ requires a rigidity resolution of

$\dfrac{\sigma_R}{R} \approx \dfrac{1}{700}$ at $R \approx 2.2 GeV/c$, and a velocity resolution of $\dfrac{\sigma_\beta}{\beta} \approx 9 \times 10^{-4}$ at $\beta = 0.62 \sim 0.66$. The latter corresponds to timing resolution of $\sigma_T \approx 50 psec$ for 10 meters of flight path, which is marginal using our current technology. Obtaining a rigidity resolution of 1/1000 requires a combination of high-field magnet and precise position-measuring detectors. The required rigidity resolution for invariant-mass measurements is smaller than that required by PID.

Summary

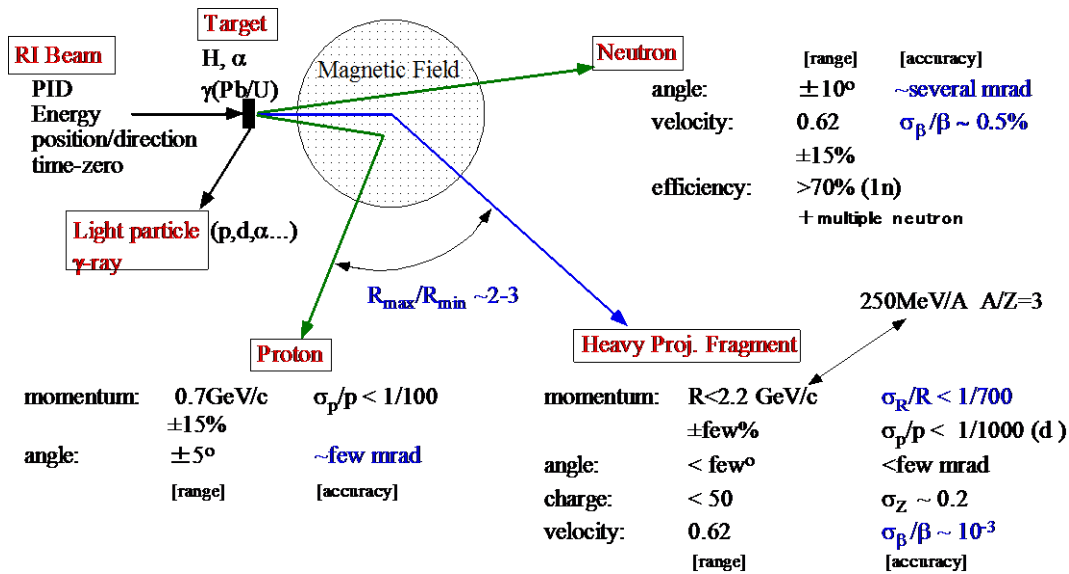Summary of required measurements is shown in Fig. 1-3-1.

Fig. 1-3-1: Summary of required measurements

Detector configuration can be modified to fit various measurements as schematically shown in Fig. 1-3-2.
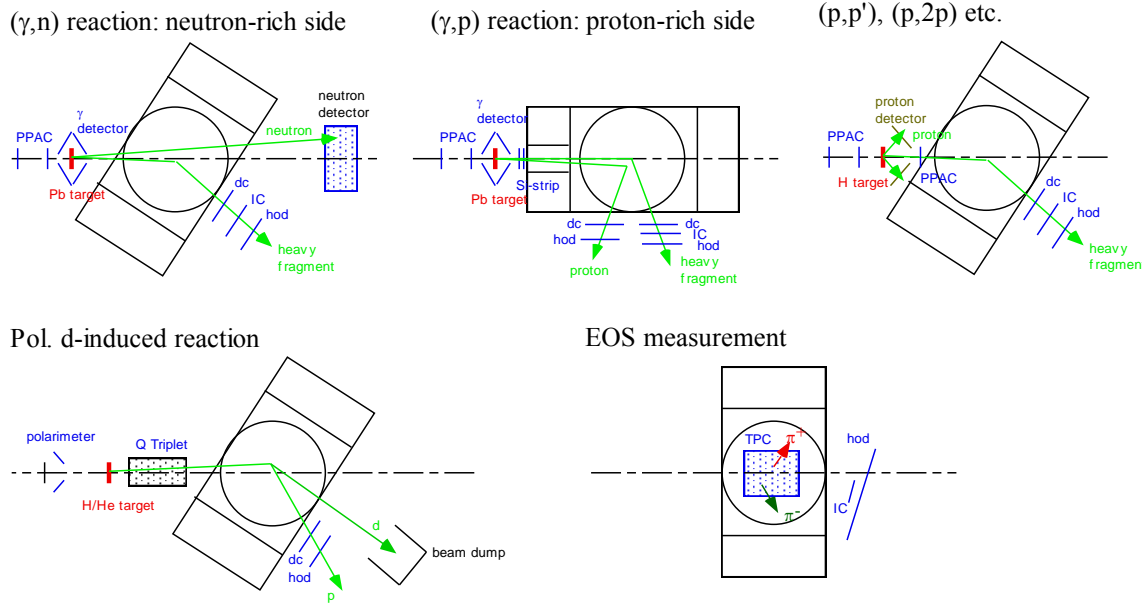
Fig. 1-3-2: Experimental setup for various configurations

Momentum resolution for polarized deuteron beam experiment

The required momentum resolution for 880 MeV deuteron is 1/1600 for good background suppression. The solid angle required is $\Delta\Omega \sim 6$ msr. In addition, well-shielded beam dump is necessary.

(γ,n)-type invariant-mass measurement

The (γ,n)-type measurements require good relative energy resolution, high efficiency, and muti-neutron detection capability. The required relative energy resolution is about 0.3 MeV at relative energy of 1 MeV. Large angular acceptance is necessary for the detection of neutrons emitted in the breakup reactions of neutron-rich unstable nuclei up to the relative energy of 8 MeV. The intrinsic detection efficiency should be higher than 60% for 1n detection and 20% for 2n detection. Capability of multi-neutron detection is also required.

(γ,p)-type invariant-mass measurement

To achieve the relative energy resolution of 0.2 MeV at 1-MeV decay energy, opening angle between a heavy fragment and proton should be less than 4 mrad resolution, with the 0.2% resolution for the momentum of the heavy fragment and 0.8% resolution for the momentum of the proton. Most marginal quantity for the relative energy resolution is the opening angle. A precise measurement of the opening angle can be achieved using silicon detectors with fine pitch strip electrodes. This detectors must be able to detect the proton and the heavy fragment with Z~50. Detectors for the proton at downstream of the SAMURAI magnet should be measure the position with 1 mm resolution and the angle with 2 mrad resolution to achieve the momentum resolution of 0.8%. And the detector size must be large enough to cover the space broadening of the proton due to the strong focusing by the magnetic field. The size will be larger than 1.5 m wide and 80cm height. To measure the multi proton-emission events, the detectors must be able to handle the multi-proton hit. To maximize the detection efficiency of the coincidence measurement of the heavy fragment and protons, the SAMURAI magnet should accept the wide

momentum of $R_{\max}/R_{min} \approx 2 \sim 3.$

EOS study using SAMURAI TPC

The SAMURAI TPC must accurately measure minimum ionizing p, π^+ and π^- in the presence of a projectile-like residue and a large multiplicity of intermediate mass fragments (IMF's) as large as 80. We can realize such performance based on the design of EOS TPC. To match to its pole diameter of 2 m and available magnet gap of 80 cm we proposed the relevant parameters of the proposed SAMURAI TPC as listed in Table 1-3-1.

SAMURAI TPC Parameters	
Pad Plane Area	1.3 m x 0.9 m
Number of pads	11664 (108 x 108)
Pad size	12 mm x 8 mm
Drift distance	55 cm
Pressure	1 atmosphere
Gas composition	90% Ar+10% CH_4
Gas gain	3000
E field	120 V/cm
Drift velocity	5 cm/µs
dE/dx range	Z=1-8, π, p, d, t, He, Li-O
Two track res.	2.5 cm
Multiplicity limit	200

Table 1-3-1: Parameters of the SAMURAI TPC

[2] SAMURAI Spectrometer: Description, Current Status, and Construction Plan

[2-1] Superconducting Dipole Magnet

H. Sato[*], K. Kusaka, J. Ohnishi, H. Okuno, T. Kubo (RIKEN)

[2-1-1] Design policy (requirements)

A large-gap superconducting dipole magnet is a central part of SAMURAI spectrometer. The following list contains the requirements on the dipole magnet.

From the experimental side:

- Large fields integral: for high precision momentum analysis.
- Large pole gap: for large vertical acceptance for neutrons.
- No coil link: for large acceptance in the horizontal direction.
- Small fringing field: for detectors around the target region and tracking detectors.
- Flexibility: for various experimental configurations.
- Large momentum acceptance: for heavy fragments and protons in coincidence.
- High momentum resolution: for deuteron-induced reactions.

From magnet construction:

- Simple structure: H-type magnet, round coil.
- Cooling system similar to STQ: proved technology.

Out of various designs, the following parameters are selected:

- H-type superconducting magnet with a round pole, for simple structure.
- Field integral of 7 Tm, providing rigidity resolution of 1/700 (rms) at 2.3 GeV/c, and particle identification up to A=100.
- Vertical gap of 800 mm, providing vertical angular acceptance of ±5 degrees for projectile-rapidity neutrons.
- Rotatable base from -5 to 95 degrees, for various experimental configurations.
- Field clamp, to minimize the fringing field.
- Built-in vacuum chamber with flanges, for effective usage of the magnet gap.
- Holes in the return yoke, for detecting projectile rapidity protons and heavy fragments in coincidence with R_{max}/R_{min}=2~3.
- Q3D option for high-resolution measurement. A last triplet Q magnet in the beam line is used with the dipole magnet in the Q3D mode, providing momentum resolution of 1/3000.
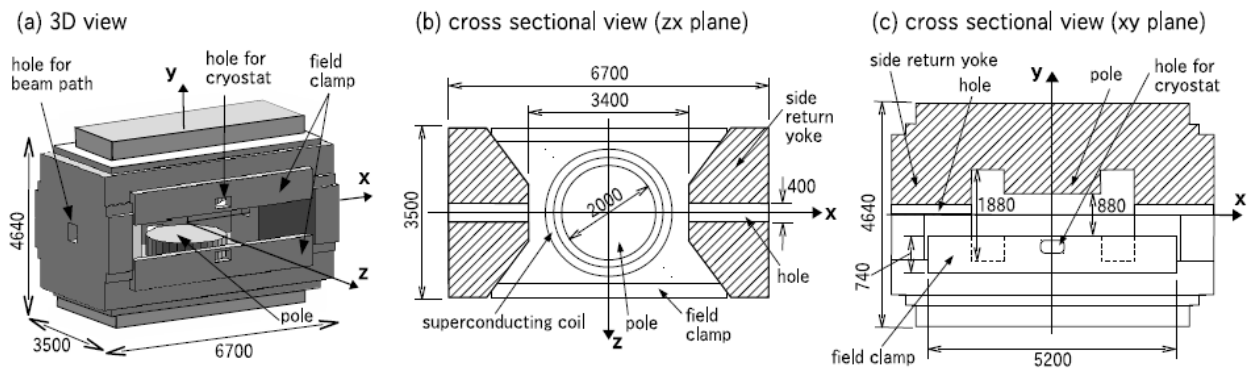
Fig. 2-1-1: Schematic view (a) and cross sectional views (b)(c) of the SC dipole magnet of the SAMURAI spectrometer.

[2-1-2] Outline of the superconducting dipole magnet

  The main parameters which are set by taking into account the requirements listed above are shown in Table 2-1-1 and Table 2-1-2. The magnet is a H-type dipole, having cylindrical poles of 2 m in diameter and round superconducting coils. The upper and lower superconducting coils are installed in their each cryostat, and cooled separately by liquid helium bath cooling method. Figure 2-1-1 shows a schematic view and cross sectional views of the dipole magnet. The maximum magnetomotive force is 1.9 MAT/coil, which generates a magnetic field of about 3.1 T at the center of the poles in the median plane. The magnet is designed to have a maximum bending power (BL integral) of 7 Tm.

Table 2-1-1: Electro-magnetic parameters

	value
type	H-type, superconducting
current	560 A
magnetomotive force	1.9 MAT/coil
current density of coil	66.0 A/mm^2
field at the pole center (median plane)	3.1 T
BL integral at 3.1 T	7.05 Tm
maximum magnetic field in a coil	5.26 T
inductance	212 H
stored energy	33 MJ

Table 2-1-2: Geometry of the magnet

	value
pole shape	circular
pole gap	880 mm (800 mm in vacuum chamber)
pole diameter	2000 mm
pole height	500 mm
yoke width	6700 mm
yoke depth	3500 mm
yoke height	4640 mm
yoke weight	566140 kg

[2-1-3] Magnetic field calculation

Figure 2-1-2(a) shows excitation curves of the dipole magnet. The points with a solid line are calculated values by using the code TOSCA, while the dotted straight line is obtained by assuming that the magnetic permeability of iron is infinity. The y component of the magnetic fields $B_y(z)$ obtained with the magnetomotive force of 1.9 MAT/coil is shown along the z-axis in Fig. 2-1-2(b). Note that the definition of the coordinates is given in Fig. 2-1-1. The integration of $B_y(z)$ for the region from z=-2 to +2 m is calculated to be 7.05 Tm, which fulfills the requirement of bending power.
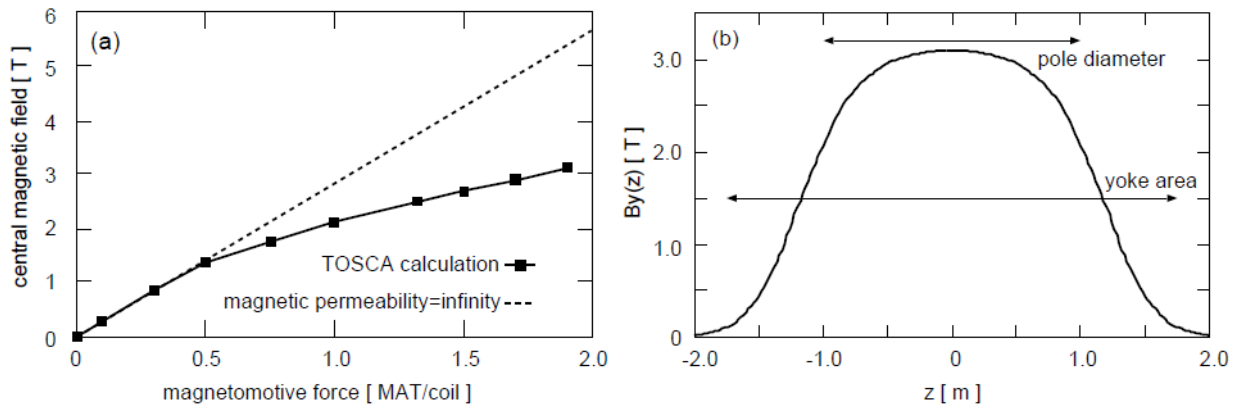
Fig. 2-1-2: (a) Excitation curve. (b) y component of magnetic field $B_y(z)$ plotted along z-axis.

For accurate magnetic rigidity (momentum) measurements, particles should not be bent much by magnetic fringing fields in the area where the tracking detectors are placed. Thus it is important to estimate a shape and a magnitude of the fringing field distribution and reduce it by adjusting the dimension of the magnet. We attempt to minimize the fringing fields by optimizing the dimension of the return yokes and the field clamps (Fig. 2-1-1).

In order to reduce the fringing fields, we checked the influence of the thickness of the field clamps.

Figure 2-1-3(a) shows the $B_y(z)$ distribution along the z-axis in the fringing field region obtained with the magnetomotive force of 1.9 MAT/coil. The fringing fields become smaller as the field clamps become thicker, as anticipated. In order to optimize the thickness, we calculated the integration of $B_y(z)$ along the region of 2.2 m < z < 5.0 m, where the tracking detectors are placed. Figure 2-1-3(b) shows the result of the integration *BL*. The optimal thickness of the field clamps was determined to be 250 mm, in which the *BL* shows a minimum value.
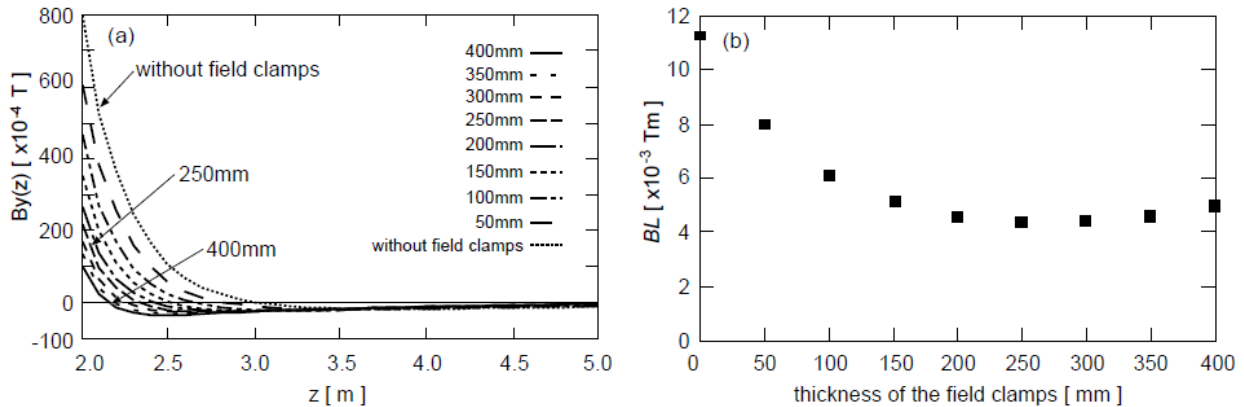
Fig. 2-1-3: Fringing fields calculated for different thickness of the field clamps: (a) distribution of $B_y(z)$ along the z-axis, (b) integrated values *BL* from z=2.2 m to 5.0 m.

Figure 2-1-4 shows the $B_y(z)$ distribution calculated for different central magnetic fields. In the case of maximum field, 3.1 T (1.9 MAT/coil), the peak value of the fringing fields was calculated to be -2.6×10^{-3} T. This value is acceptable to achieve the required magnetic rigidity resolution.

Fig. 2-1-4: $B_y(z)$ in the fringing field region for different magnetic fields.

[2-1-4] Superconducting wire, coil structure and cryocooler system

   We use a conventional NbTi superconducting wire. The properties of the NbTi wire are listed in Table 2-1-4. Geometry of a coil is also shown in Table 2-1-5. The outer layer of the coil is surrounded by heater of copper wires. When the cooling system controller detects quench, a protection switch is opened 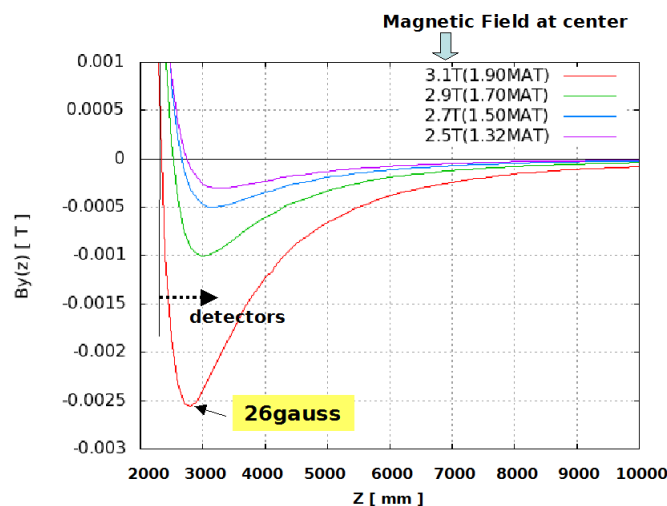and a closed circuit is formed, which consists of the coil, diodes and heater. Quench heater is used to protect the coil by greatly increasing the coil normal zone. And then stored energy is spent by increase in temperature of the superconducting coil (Fig. 2-1-5). It is estimated that the coil becomes 110 K in average and quench point becomes 160 K after 30 seconds from quench.

Table 2-1-4: Parameters of SC wire

	value
material	NbTi/Cu
diameter	3mmϕ
Cu/SC ratio	5.0 ~ 6.0
insulation	PVF (> 40 μm)
filament diameter	~ 28 μmϕ
number of filaments	~ 1760
twist pitch	~ 88 mm
RRR	> 100
critical current at 4.2 K	> 4000 A at 3 T
	> 3290 A at 4 T
	> 2690 A at 5 T
	> 2150 A at 6 T

Table 2-1-5: Geometry of the coil

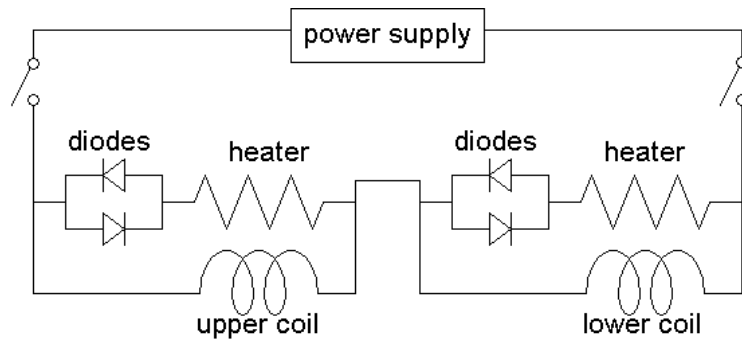|	value
number of turns	3411 turns/coil
coil inner diameter	2350 mm
coil outer diameter	2710 mm
coil cross section	180 x 160 mm^2
coil weight	1783 kg/coil

Fig. 2-1-5: Quench protection circuit for superconducting coils.

The upper and lower superconducting coils are installed in separate cryostats, and cooled by a cryocooler system mounted on each cryostat. There are no coil links between the coils. A schematic view of the coil is shown in Fig. 2-1-6. Each coil is equipped with two 4 K GM-JT cryocoolers which re-condensate evaporating liquid helium. The helium vessel which accommodates the SC coil is surrounded by 20 K and 80 K thermal shields cooled by four GM cryocoolers. There is also a GM cryocooler for each coil, which is used to cool current leads made by high-T_c superconductor Bi2223. In total, there are 14 cryocoolers for the superconducting dipole magnet (Table 2-1-6). This cryocooler system is similar to that of STQs of BigRIPS. Then the system will be reliable.

Table 2-1-6: Cryocoolers

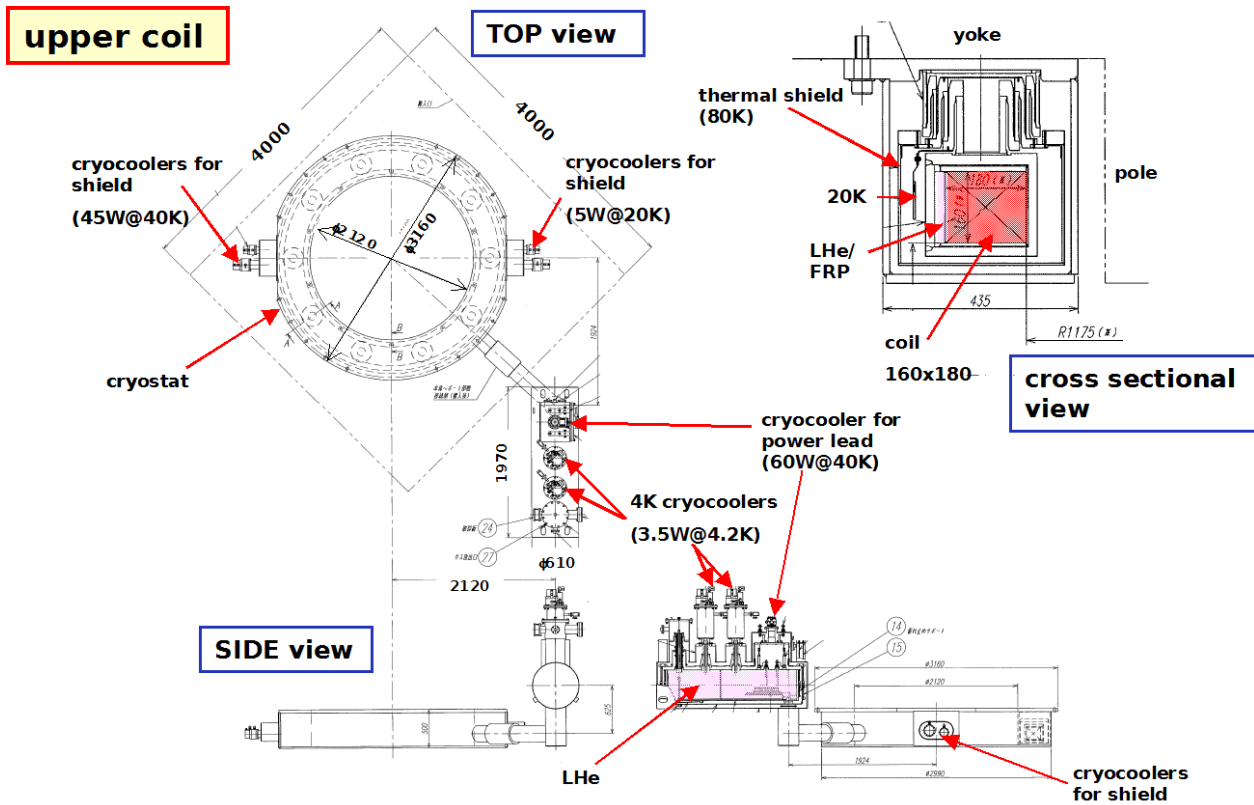|	liquid-He vessel	thermal shield		current lead
		20 K	80 K	
cryocooler	GM-JT x 2	GM x 2	GM x 2	GM x 1
cooling power	3.5 w @4.3 K	5.0 W @ 20 K	45 W @40 K	60 W @40 K
heat load	4.11 W	4.96 W	78.22 W	53.94 W

Fig. 2-1-6: Schematic views of the cryostat for upper coil with the cryocooler system.

[2-1-5] Geometry markers

  Position detectors for SAMURAI have to be well located upstream and downstream of SAMURAI magnet. Typical position determination accuracy of these detectors is order of 100 μm (RMS). In order to obtain sufficient momentum resolution of the particles in the experiment, these detectors have to be well arranged within 10 μm preferably or 50 μm in the worst cases. In order to place them accurately and efficiently, we plan to introduce photogrammetry system. This system realizes the position reconstruction within 25 μm or better by multiple numbers of pictures taken by a single lens reflex camera with well calibrated lens optics. This system requires us to prepare the target markers to be taken by the camera. More specifically, the corner cubic reflectors or compatible items have to be deployed on several positions of the magnet and also the detectors. In the same time, TOSHIBA plans to use a laser tracker system to build the magnet and the vacuum chamber. This system also enables them to obtain accurate position in real time. Comparison of these two systems is summarized in Table 2-1-7.

Table 2-1-7: Comparison of laser tracker and photogrammetry.

Items	Company	Method	Latency	Calibration	Sense of usage
Laser tracker	Leica	Laser Interference	real time	Complicated	Professional
Photogrammetry	TACC	Parallax	1-10 min.	Not so complicated	user friendly

The geometry markers are layout on the 15 positions on the magnet yoke and field cramp indicated in Fig. 2-1-7. These target markers positions will be measured on the construction of the dipole magnet by TOSHIBA. The geometry relative to the gap center will be given from the measurement using the laser tracker system. Afterwards, in-house collaborators or users can put experimental instruments accurately with referring the target marker positions using the photogrammetry system. Detail description of the photogrammetry system can be obtained at URL : http://www.geodetic.com/whatis.htm .   In addition to the layout of the detectors, the photogrammetry system can be utilized for accurate rotation angle determination of SAMURAI magnet and for monitoring the displacement of the magnet or vacuum chambers with finite aging.

The magnet yoke has also lines of reference at vertical and horizontal center (Fig. 2-1-8). These lines are used to check roughly the alignment of the magnet with optical scope such as transit. The lines will be marked after finishing a construction of the yoke.

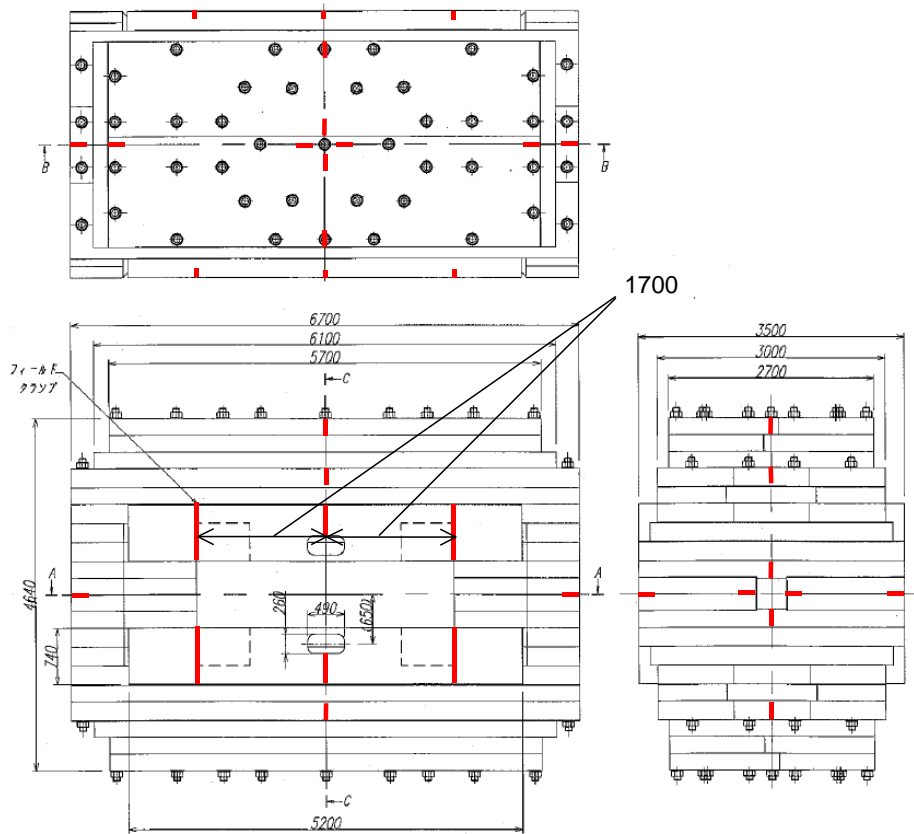Fig. 2-1-7: Positions of the geometrical markers.

Fig. 2-1-8: Positions of the lines of reference.

[2-1-6] Current status of the construction of the superconducting dipole magnet

Construction of parts of the magnet has started in TOSHIBA. A coil wiring, casing into the cryostat have been already finished (Fig. 2-1-9). Iron blocks for the yoke were also prepared in TOSHIBA. The construction at RIBF site will start in October 2010 and finish in May 2011. For the construction at RIBF site, the SAMURAI pit was set as an independent area by surrounding new walls, brocks and doors. Then, we can proceed the construction during beam time. A construction timeline of the magnet is shown in Table 2-1-8.
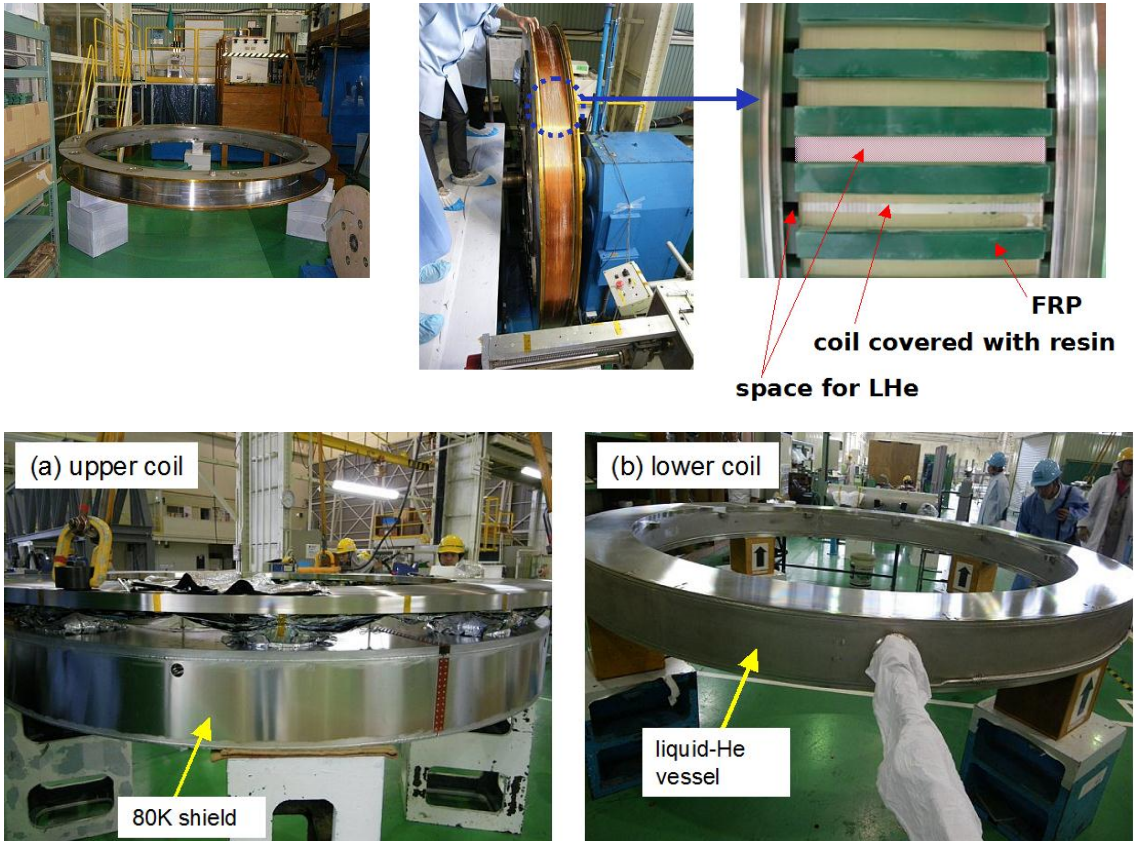
Fig. 2-1-9: Photos of the coils, taken at TOSHIBA factory.

Table 2-1-8: Construction timeline of the dipole magnet.

	2010			2011				
	Oct.	Nov.	Dec.	Jan.	Feb.	Mar.	Apr.	May
rotatable base	■	■						
yoke construction		■	■					
cryostat (coil) installation				■				
chamber installation					■			
cryocooler, compressor					■			
power source, electric line				■	■	■		
leak test						■		
cooling test							■	
excitation test							■	
stage construction								■

[2-2] Superconducting Triplet Quadrupole Magnet (STQ25)

H. Sato[*], K. Kusaka, J. Ohnishi, H. Okuno, T. Kubo (RIKEN)

[2-2-1] Design and placement of STQ25

A SC triplet quadrupole magnet (STQ25) is placed in front of the SAMURAI dipole magnet. It is used not only in the normal beam focus mode but also in the Q3D mode, providing momentum resolution of 1/3000 in pol-d experiments. A design of STQ25 is same as recently introduced STQs in BigRIPS. It has three SC quadrupole magnets Q500-Q800-Q500 and one sextupole magnet SX. The electro-magnetic specifications of STQ25 are shown in Table 2-2-1.

Table 2-2-1. Magnetic parameters of STQ25.

	value
type	super-ferric
Q500,800: magnetic gradient	14.1 T/m
Q500,800: magnetomotive force	190 kAT/coil
Q500,800: number of turns	1403 turns/coil
Q500: current	142 A
Q800: current	137 A
SX: magnetic gradient	15 T/m^2
SX: magnetomotive force	28.2 kAT/coil
SX: number of turns	580 turns/coil
SX: current	48.6 A

STQ25 is put on the stage which can move along the beam line. Movable distance is 2.5 m. So we can choose the best optics for each experiments by optimizing the position of STQ25 (Fig. 2-2-1).

[2-2-2] Current status

  We are now preparing a contract with TOSHIBA for lease of STQ25 and the movable stage. They will be delivered in February 2012.
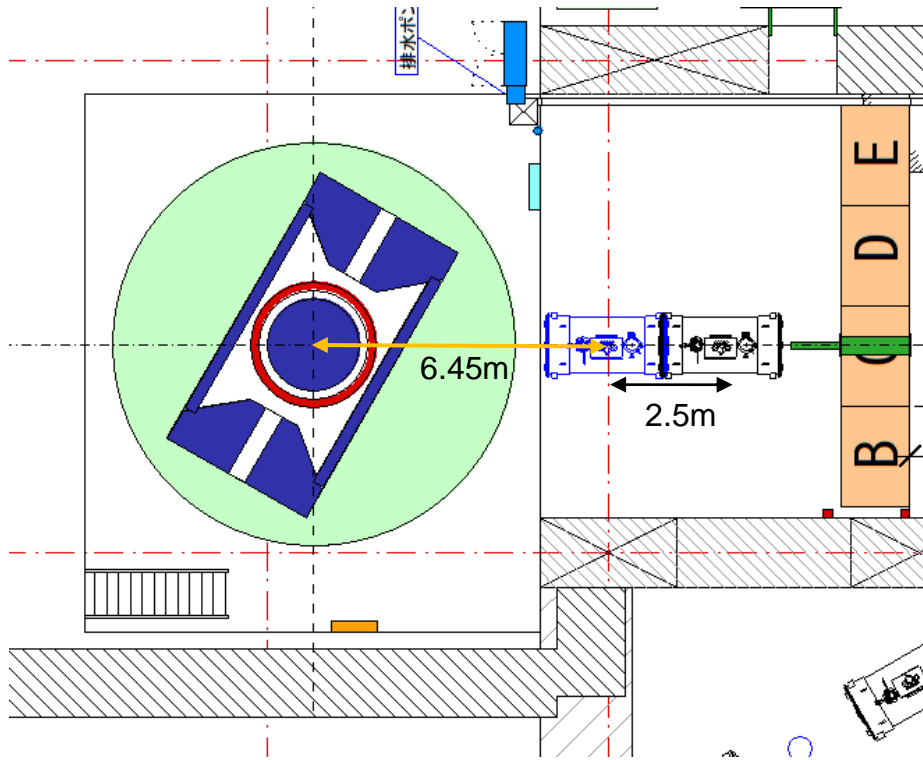

Fig. 2-2-1. Placement of STQ25. The optimum position is now studying.

[2-3] Vacuum System

H. Otsu[*], Y. Shimizu (RIKEN)

Vacuum system is one of the most important infrastructure for nuclear physics experiments to provide primary or secondary beam particles on target and to measure scattering particles without being disturbed by materials for energy deposit or multiple scattering. In this sense, whole system including detectors for position, timing, energy deposit, or total kinetic energy measurement had better to be placed inside vacuum. On the other hand, it will be much easier when those detectors are located outside vacuum, i.e. in the air circumstance from a point of view of signal handling, high voltage supplying or operation of preamplifiers. So, we have to compromise the vacuum system depending on the experiment to be done, especially on the region of mass numbers.   Planned experiments using SAMURAI spectrometer are so-called "one-path" experiments where beam or scattered particles pass through for one time. So, typical required vacuum is expected to be order of 10^{-6} Torr.

In this section, design policy of vacuum system, geometry of vacuum layout, and present status are described followed by a timeline in near future. Report of test of an exit window with large area is added.

[2-3-1] Design policy for vacuum instruments

SAMURAI spectrometer is designed to provide a variety of nuclear physics experiments as are described in the chapter 1.   Five categorized experiments are schematically drawn in Fig. 1-2-2. Vacuum instruments are also expected to be layout depending on the experimental requirement as well as possible. In a designing phase, common instruments were distinguished from other instruments required by individual experimental setups. The common instruments are 1) beam line, 2) magnet gap chamber, 3) vacuum pumping system. Individual instruments are considered to be 4) target chamber, 5) upstream connection flange, 6) downstream connection flange, and others which are needed in the other configurations. Depending on the experiment, vacuum windows for heavy ions, neutrons and protons are needed.

Focusing on the magnet gap chamber, two different species of particles are passing through on downstream with spatially separated manner depending on experimental setups as:

i) neutrons for left side and heavy ions for right side on the (γ,n) type experiments,

ii) heavy ions for left side and protons for right side on the (γ,p) type experiments,

iii) leading particles and other lighter particles on the missing mass measurements,

iv) beam deuteron and scattered particles on high resolution mode for few body system studies.

The downstream end flange had better to be divided into two separate flanges which will be extended to detectors or be closed by vacuum partition windows. Of course single large window will be needed for some experimental configuration. So, two-window flange are attached on the exit flange of the gap vacuum chamber. In the same manner, another two-window flange are attached on the entrance flange of the gap vacuum chamber.   Details will be given later.

[2-3-2] Geometry of the vacuum system

Beam line

For the beam line, a target chamber at F13 to be designed have to be connected with vacuum duct from an existing vacuum chamber at F12. Distance between two ports is 15.2 m. Beam duct size is compatible with JIS 250, outer diameter of 267.4 mm, which is the same size of upstream beam duct. At present STQ25 will be replaced on the beam line just upstream of the target chamber. A stand for STQ25 is designed to be adjustable or movable along to beam direction denoted as a Z axis. Vacuum duct should be adjusted depending on the place of STQ25.

Magnet gap section

Vacuum chamber inside the magnet gap is most important instrument of the vacuum system on SAMURAI. Fig. 2-3-1 shows the geometry of the vacuum chamber in the magnet gap section with the entrance and exit windows. The vacuum chamber is located on the center region of the magnet gap and tapered to downstream along to the magnet return yokes. The entrance region is cut off at gap inside 750 mm from outer face of field cramp in order to realize a finite angle injection up to 45 degree. The vacuum chamber is configured with 35 mm thickness stainless steel SUS304. Top and bottom faces are connected with screws on outskirts of the magnet poles in order to prevent the chamber collapsed inside by vacuum pressure. Each connecting screw is vacuum sealed individually.
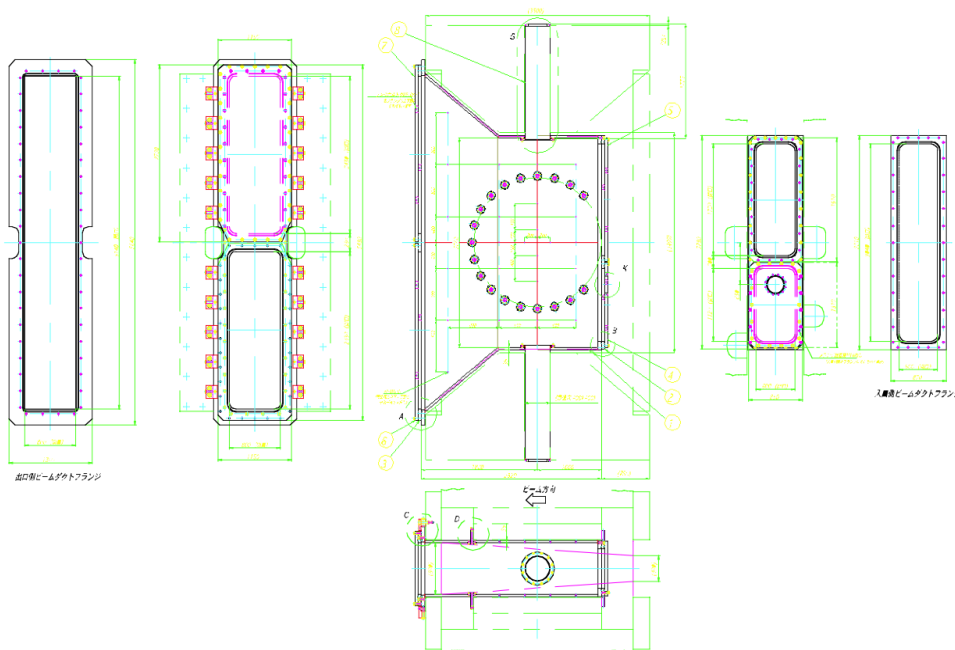

Fig. 2-3-1: Vacuum chamber geometry of the magnet gap section.

Properties of the vacuum chamber are shown in Table 2-3-1.

On the entrance window, a flange with two windows is mounted to separate between beam entrance window and vacuum pump connection window. These two windows are 300 mm offset for enlarging the beam entrance window, which enables us to adjust various configurations from 0 to 45 degrees of the

magnet relative to beam axis.

On the side faces at magnet center, two pipes with 390 mm φ toward 90 and 270 degrees are arranged. The pipe at 90 degrees is utilized for the (γ,p) type experiment with high momentum resolution mode. Scattered particles are led through the pipe to magnet center. The pipe at 270 degrees is invested to auxiliary usages. Accurate geometry calibration will be done using 90 and 270 degree pipes. A vacuum pump system is mounted here at 90 degree configuration. Laser is introduced to TPC chamber for position calibration through this pipe.

On the bottom and top face several screw holes are layout for fixing items inside the vacuum chamber. Several numbers of screw holes are also located on the side face.

On the exit window, a flange with two windows with symmetrical configuration is mounted. These two windows are used for combination of scattered particles spatially separated as heavy ions and neutrons or protons and heavy ions. The exit window flange is tightly pressed on the magnet field cramp with 90 degree gimmick of screws in order to prevent the chamber collapsed inside by vacuum pressure, especially for the downstream skirt region.

Table 2-3-1: Vacuum chamber properties at magnet gap section.

Volume	7.9 m^3
Weight	8.8 t
Material	SUS304
Thickness (side and top faces)	35 mm^t
Thickness (flange)	60 mm^t
Entrance cross section (inner)	3240×800 mm^2
Straight section	1560 mm
Skirt section	1140 mm
Exit cross section (inner)	5140×800 mm^2
Entrance window	3040×600 mm^2
Beam entrance window (right)	1720×600 mm^2
Vacuum pump window (left)	1120×600 mm^2
Exit window	5140×800 mm^2
Exit window (left)	2430×800 mm^2
Exit window (right)	2430×800 mm^2
Center structure	280 mm$^w \times$ 50 mm^t
Side pipe cross section	390 mmφ (outer), 4.5mm^t
Side pipe length	1720 mm from outer face

Vacuum pumping system

Four sets of vacuum pumping systems are prepared and ready. Two of them consist of 1100 l/s TMP followed by a rotary pump and two vacuum gauges covering from low vacuum to 10^{-6} Torr or lower. The other two consist of 2300 l/s TMP with the same peripherals. The vacuum pumping systems with the 1100 l/s TMP will be mounted on beam line and target chamber. The two of 2300 l/sec systems will be mounted on the gap vacuum chamber from upstream and downstream, respectively. The layout will be changed depending on vacuum chamber layouts, especially for the second 2300 l/sec pump station.

Two examples for 30 degree setup and 90 degree setup are also shown as cross section views of 3 dimensional CAD descriptions. For (γ,n) type experiments, the second vacuum pump station will be mounted beneath of the extension chamber. For (γ,p) type, and others where no extension chamber is needed, the second vacuum pump station will be mounted on the auxiliary port.
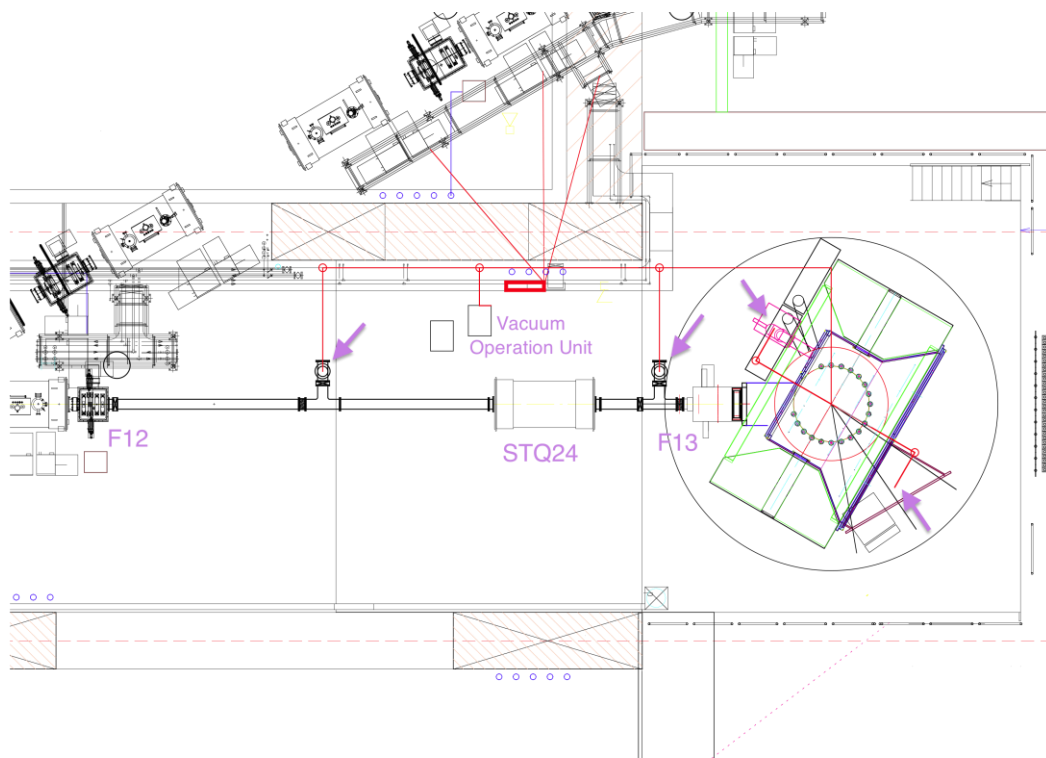

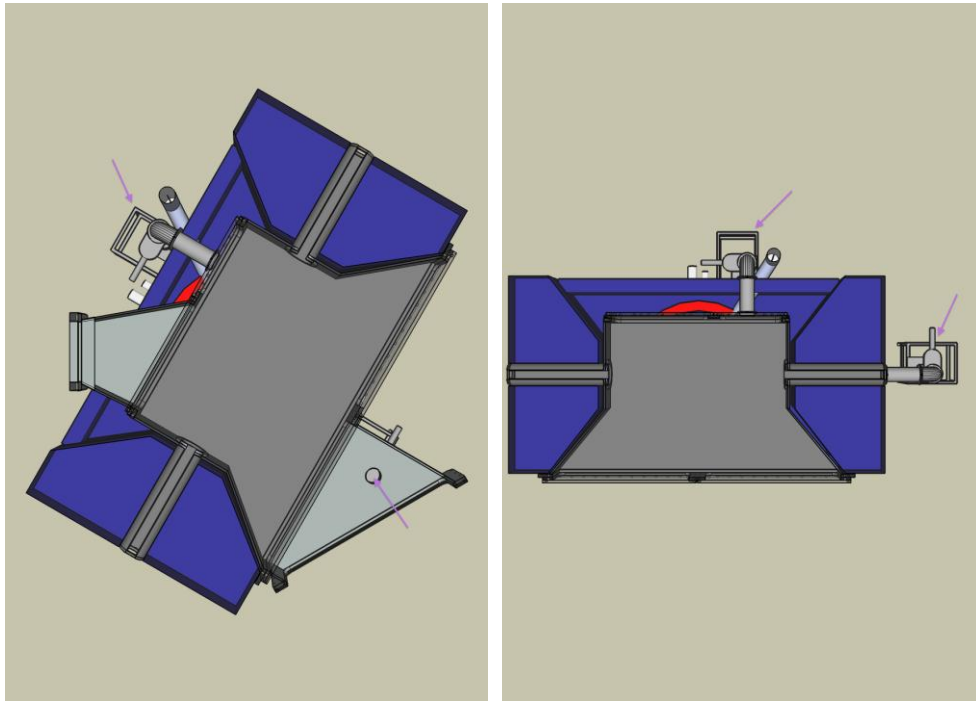Fig. 2-3-2: Layout of four vacuum pumping systems.

Fig 2-3-3: Two examples of the vacuum pumping system layout.
(Left) 30 degree configuration. (Right) 90 degree configuration.

Target chamber

Target chamber configuration will be changed depending on the experiments. Beam line detectors, target itself, and FDC1 are contained in the target chamber. For studies for heavier isotopes, the target section has better to be covered by a γ ray detector array because residual particles do not always stay on ground state. Detail designing for early phase of experiments will be started soon.

Upstream connection section

Downstream of the target chamber, a gate valve and a connection duct are located to connect vacuum to the entrance window of the vacuum chamber at the magnet gap section. Scattered particles pass through this section except the EOS measurement. So, connection duct have to be designed to cover as much solid angle as possible for the scattered particles. The shape of the connection duct has to be adjusted depending on the magnet angles. At present, 30 degrees is used for the (γ,n) type experiments. For the (γ,p) type, missing mass measurement, larger angles are preferred. It is not well determined that 40 degrees or 45 degrees are more preferable. For EOS experiments, SAMURAI magnet is set with 0 degrees or smaller angles. In this case, beam particles pass through this section. The connection duct size will be comparable with the beam line upstream. Between the target chamber and upstream connection duct, we plan to separate vacuum section with a large rectangular gate valve.
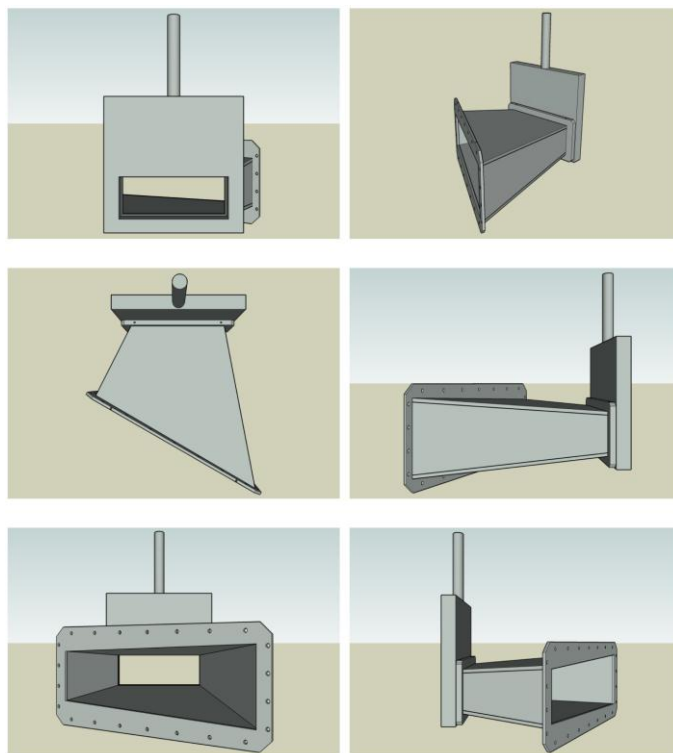
Fig. 2-3-4: Upstream connection duct for 30 degree configuration.
A large rectangular gate valve is mounted.

Downstream connection section

In order to maximize the performance of FDC2, FDC2 should be layout on perpendicular geometry with particle trajectories as well as possible. Supposing to detect 60 degree bending heavy ions on 30 degree configuration, additional 30 degree flange enables us to inject particles on the position sensitive detectors FDC2 with the perpendicular direction on central trajectory. For this purpose downstream extension duct is needed especially for the (γ,n) type experiments. The extension duct may also be helpful for other type of experiments. FDC2 has been considered to place in the vacuum circumstance or in the air by partitioning with thin foil window from vacuum. Both of them have advantages and disadvantages. Vacuum circumstances will provide higher momentum resolution while air circumstances make system simple and vice versa. The extension duct is being designed to fit with the both configuration. The schematic view is shown in the left flame of Fig. 2-3-3.

Vacuum partitioning window

The vacuum area and air have to be separated by vacuum partitioning windows for neutrons and charged particles, which are triggered by plastic scintillator hodoscopes located on the air circumstance.

For neutrons, it is required to realize lower reaction losses of beam rapidity neutrons on the partition window material. In the same time the window have to support itself with sufficient strength. The area to be covered is 2430×800 mm^2. The amount of the window materials and substances is being considered by referring existing examples like that of the ALADIN spectrometer at GSI. They use the steel with 4.5 mm thickness and 1200 mm square. The steel material is processed to form a tail end shape of the gas tank.

For charged particles, it is required to realize lower multiple scattering and lower energy loss difference for beam rapidity heavy ions on the partition window foil material. The area to be covered is 2800×800 mm^2. The window material makes penetrating particles deflect by multiple scattering and makes them energy fluctuation by energy losses. Required momentum resolution of 1/700 gives upper limit of the amount of the material as radiation length of $L/L_R \sim 10^{-3}$. In the same time, it is necessary to ensure the strength to hold vacuum. Details to test of the charged particle window are given in later in section 2-3-4. In this series of efforts, the exit window of the LAS spectrometer in RCNP is mainly referred. The size is 2 $\times$ 0.4 m^2 and material is a combination of Kevlar and Mylar. If the window is realized, that may be utilized for the neutron window.

[2-3-3] Present status of the vacuum instruments

The vacuum chamber at gap section with entrance and exit window flanges is in construction based on Toshiba's responsibility. The vacuum chamber will be fabricated in the same timing of fabrication of the dipole magnet. RIKEN has responsibilities on upstream and downstream sections. Now in-house members in SAMURAI group are concentrated on the 30 degree configuration for upcoming experiments on earliest phase of end of FY2011. The beam line and STQ25 section will be constructed on former half of FY2011. The upstream connection duct and the downstream extension duct will be finally designed soon and fabricated on the end of FY2011. These instruments are shown as bird eye views in Fig. 2-3-5. We soon start to design the target chamber for the γn experiments with 30 degree configuration. The vacuum partition window is under study for feasibility, which is given in section 2-3-4.

For the next phase of experiments after FY2012, it is needed to prepare instruments for various experiments. Another upstream connection duct for 40 or 45 degree configuration has already designed. The period for fabrication and installation is not yet determined. Target chambers and connection ducts for γp, missing mass and deuteron induced experiments will be designed in midst of FY2011. The timing is not clearly determined but following instruments will be designed in FY2011-2012 :

Upstream connection duct for EOS TPC configuration,

Downstream beam duct for primary deuteron beam to beam dump,

FDC2 outer case connection,

and so forth.

These items will be developed and constructed by collaboration among each experimental group and in-house members in SAMURAI group.
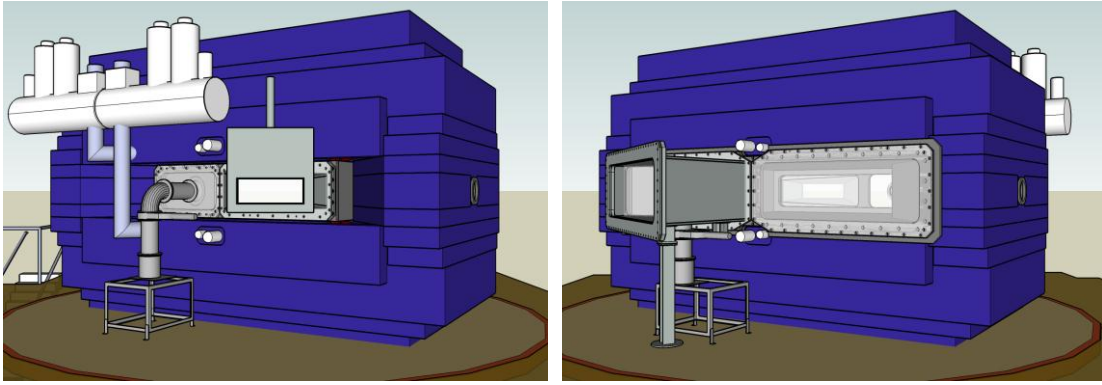
Fig. 2-3-5: Bird views for the vacuum chamber of 30 degree configuration
from upstream (left) and downstream (right).

[2-3-4] Test of large exit window

Trial foil

Vacuum window foil for trial consists of Kevlar fiber textile for supporting pressure and polyethylene foil for vacuum separation. From vacuum side to air circumstance, Kevlar textile and polyethylene foil are ordered. The Kevlar textile made of K49 fiber called as #500. The weight per unit area is 163 g/m^2. The thickness is accounted to 0.28 mm. The reason of the selection is that roll of the textile with 1420 mm width are available on a commercial basis. Polyethylene foil with 100 μm is also selected because of availability. On the contrary, the polyethylene foil is very easy to be defeated by being scratched. If some of commercial maker provided a roll of Mylar or Kapton foil with more than 1200 mm width, we would choose them.

Test using the trial foil

At present, the foil combination is in test whether it can support the vacuum sufficiently. The geometry of the test vacuum chamber window is 2800×1000 mm^2, which is about 20 % larger in length than those of the real exit window. Window support flames are made of aluminum A5650 with 3050×1250 mm^2 of area. The trial foil is sandwiched by the window support flames.   O ring can be attached on the vacuum side of the window support flame.   Several conditions have been tested as just sandwiched without gluing, glued with 4mm or 30 mm width of Araldite, add additional glue between polyethylene and Kevlar textile. Tentative results are summarized in the Table 2-3-2.

Table 2-3-2: Tentative results of foil test.

Condition	Achieved vacuum	Comment	Date
Without gluing	420 mbar	leak	2010/4/12
Gluing, 4mm width	300 mbar	collapse	6/3
Gluing, 30mm width	240 mbar	leak	6/26
Gluing, 30mm width, polyethylene also glued	100 mbar	leak	7/23

From practical point of view, it was found that the most important point is to fix the Kevlar textile on the window flame with gluing more than 30 mm width. When the gluing is not sufficient and several part is removed from the window flame, collapse occurred. When collapse occurred in the real SAMURAI configuration, almost all instruments would be damaged including upstream accelerator. So, important point to support vacuum pressure is gluing the Kevlar textile sufficiently. The rest problem is achieved vacuum pressure. From now on, the achieved vacuum rate is still 100 mbar. Vacuum leak is considered to have occurred on screw holes through Kevlar textile. Fig. 2-3-6 shows vacuum leakage after a vacuum pump was stopped. Achieved vacuum pressure was completely determined by leakage. So, we have to take more care for leakage path when gluing the trial foil on the window flame. As a next step, arrangement of gluing at inner region of the screw holes are considered and prepared in order to realize much better achieved pressure. The final goal of this trial is to achieve pressure of 10^{-6} Torr, while we have to improve and confirm methods step by step.

Window shape of vacuum phase is shown in Fig. 2-3-7 at the trial on Jul. 23rd, 2010. The window was shaped as vacuum made better. The maximum displacement on the center region was approximately 20 cm at the achieved pressure of 100 mbar. It is expected that the window shape on pressure lower than 1 mbar is almost same with that of 100 mbar.
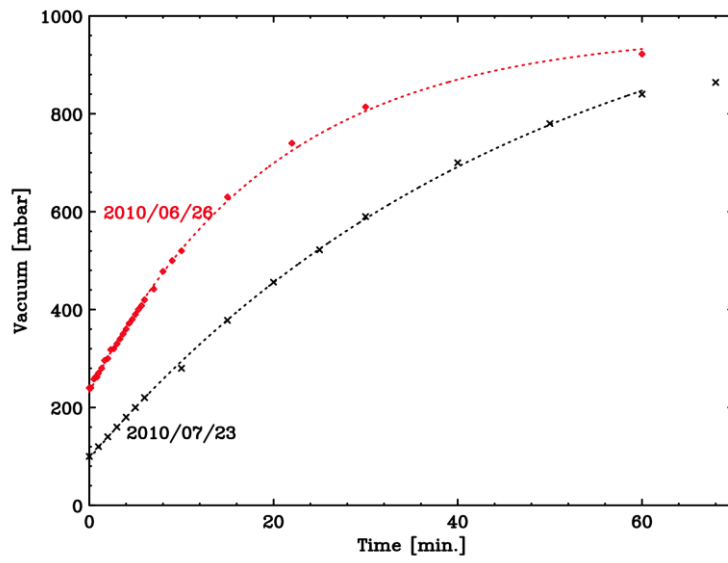
Fig. 2-3-6: Vacuum leakage after stopping pumping. Condition at the trial on Jul. 23rd was much better than that of previous trial. Improved gluing would realize better achieved pressure.

Fig. 2-3-7: Shape of the vacuum window at 100 mbar. Distance to the deepest face is about 20 cm.

[2-3-5] Schedule Plan

Our schedule plan until commissioning machine time is summarized in Table 2-3-3.

Table 2-3-3: Schedule plan until commissioning machine time.

Material	Usage	2010 4 — 6	2010 7 — 9	2010 10 — 12	2011 1 — 3	2011 4 — 6	2011 7 — 9	2011 10 — 12	2012 1 — 3	2012 4 — 6
Beamline	common				Design		Procurement and fabrication		Installation	
STQ25	common			Procurement and fabrication					Installation	
Target chamber	γ n exp.			Design		Procurement and fabrication		Installation		
	γ p exp.						Design			
	missing mass exp.						Design			
Upstream flange										
30 deg. Setup			Design	Procurement and fabrication		Installation				
40/45 deg. Setup					Design		Procurement and fabrication			
Gap vacuum chamber	common	Design		Assembly	Installation					
Downstream flange	γ n exp. and γ p exp.	Design			Fabrication		Installation			
FDC2 case connection	γ n exp. w/ high Z						Design			
Vacuum partition										
Test bench chamber	common for testing	Testing								
Kapton + Kevlar for HI,p	Charged particle of HI, p	Design				Procurement and fabrication		Installation		
Al (or other metal)	neutron			Design		Design	Procurement and fabrication		Installation	
Vacuum pumping system	common		Procurement			Installation and testing				

After commissioning and so-called "Day One" experiments, several vacuum instruments continue to be provided to realize various type of experiments. Required periods to be completed are summarized in Table 2-3-4 as a guideline.

Table 2-3-4: Timeline after commissioning machine time.

Material	Usage	2012 7 — 9	2012 10 — 12	2013 1 — 3	2013 4 — 6	2013 7 — 9	2013 10 — 12	2014 1 — 3	2014 4 — 6	2014 7 — 9
Target chamber	γ p exp.	to be completed								
	missing mass exp.	to be completed								
Upstream flange	40/45 deg. Setup	to be completed								
	TPC setup					to be completed				
Downstream flange										
FDC2 case connection	γ n exp. w/ high Z	to be completed								

[2-4] Detector System for Heavy Fragments

Y. Matsuda, K. Sekiguchi, N. Chiga, graduate students, T. Kobayashi* (Tohoku), H. Otsu (RIKEN)

[2-4-1] Overview

Position detectors

Beam is momentum-tagged by measureing the position at the momentum dispersive focal plane (F5). Beam phase space is measured by a set of position detectors befort the target. From the required momentum resolution and the bending power of the magnet, tracking detectors are designed to have an angular resolution of about $\sigma(x'_d) \approx 1\,mrad$, assuming that the beam positions are measured by extrapolating the beam trajectory, and that positions and angles are measured downstream of the magnet. In addition, another chamber is installed between the target and the magnet to measure the scatteering angle. In addition, This requires a low-mass chamber, much less than $L/L_R < 10^{-3}$, with a good position resolution.

Detectors for Particle Identification

Particle identification of heavy fragments requires velocity measurement or total-energy measurement in addition to the rigidity and the charge measurement. In order to have 5σ separation ($\sigma_A = 0.2$) at A=100, velocity resolution of $\sigma_\beta/\beta = 9 \times 10^{-4}$ @$\beta = 0.6$ or total energy resolution of $\sigma_E/E = 2.5 \times 10^{-3}$ is necessary. When the TOF method is used for velocity measurement, necessary time resolution is $\sigma_T = 50\,psec$ for 10 meters of flight path. Considering the necessity of a thin start detector for TOF, this method seems to be marginal.

We have considered two techniques for velocity and total-energy measurements: a Cherenkov detector operated at the total internal reflection (TIRC) for velocity measurement and pure CsI detector for total-energy measurement.

Design policy

Since all the detailed design of these detectors (i.e. all the contracts) had to be made in FY2008 due to the nature of the construction budget, design of these detectors are , more or less, conventional.

Detector Summary

There are four kinds of detector groups for heavy ion measurements.

* Position measurement
  * Beam Proportional Chamber (**BPC**): beam rigidity tagging at F5
  * Beam Drift Chamber 1, 2 (**BDC1,BDC2**) : beam phase space
  * Forward Drift Chamber 1 (**FDC1**) : scattering angle of fragments
  * Forward Drift Chamber 2 (**FDC2**) : rigidity analysis for fragments
  * Proton Drift Chamber 1,2 (**PDC1,2**) : momentum analysis for protons

* Charge measurement
   * <u>I</u>on <u>C</u>hamber for <u>B</u>eam (**ICB**) :   beam charge
   * <u>I</u>on <u>C</u>hamber for <u>F</u>ragments (**ICF**) :   fragment charge
* Velocity (& charge) measurement
   * <u>Hod</u>oscope for <u>F</u>ragment (**HODF**) :   velocity & charge for fragments
   * <u>Hod</u>oscope for <u>P</u>rotons (**HODP**) :   velocity & charge for protons
   * <u>T</u>otal <u>I</u>nternal <u>R</u>eflection <u>C</u>herenkov (**TIRC**) :   velocity for fragments
* Total energy measurement
   * <u>T</u>otal <u>E</u>nergy <u>D</u>etector (**TED**) :   total energy

* Readout electronics for position detectors

   As a readout circuits of position detectors, anode signals are converted into LVDS logic signals using Amp-Shaper-Discriminator boards (ASD, 16ch/board, gnd, GNA210) mounted directly on the detectors. ASD Power Supply modules are used to supply ±3V, threshold voltage, and test pulses : one ASD PS handles 10 ASD boards.   Logic signals are further processed by multihit TDC's (AMSC, 64ch AMT-VME TDC module) with 0.8 nsec/ch precision.

* Gas mixture for position detectors

   When detectors are operated at 1 atm, He+60%CH_4 is used.   This mixture comes from the compromise among multiple scattering, position resolution and running cost.   At low pressure, BPC, BDC, and FDC1 are operated using pure i-C_4H_{10}.

[2-4-2] <u>Beam</u> <u>Proportional</u> <u>Chamber</u> (BPC)

* Design

      BPC is used to tag the rigidity of secondary beams at the momentum dispersive focal plane F5 by measuring the horizontal position.   It is a 4mm-spacing multiwire proportional chamber with 2 anode planes.   It is housed in detector box, which is placed in the F5 vacuum chamber.   Since the momentum dispersion at F5 is ~33mm/%, 4mm-spacing provides momentum resolution of less than 0.1% (rms). BPC is shown in Fig. 2-4-1 and summarized in the table.

   Amp-shaper-discriminators (ASD) are mounted directly on the detector box in the F5 vacuum chamber. LVDS signals are timed , through the vacuum feed through, by TDC's.   Isobutane gas is used at about 20 torr for Kr, and about 200 torr for protons.

Anode	$20 \mu m \phi$ Au-W/Re
Anode spacing	2mm (2 wires are or-ed for readout)
Anode – cathode gap	5mm (5mm-thick G10)
Cathode, window	12μ m-thick Al-Mylar
Effective area	240mm (H) x 150mm (V)
Anode configuration	x1 - x2
#readout channels	64 anodes/plane x 2planes = 128anodes
Window of detector box	80μ m-thick Kapton x2
Operation gas	i-C_4H_{10} at 20 to 200 torr
HV	cathode
Readout	ASD x8, ASD PS x1, TDC x2
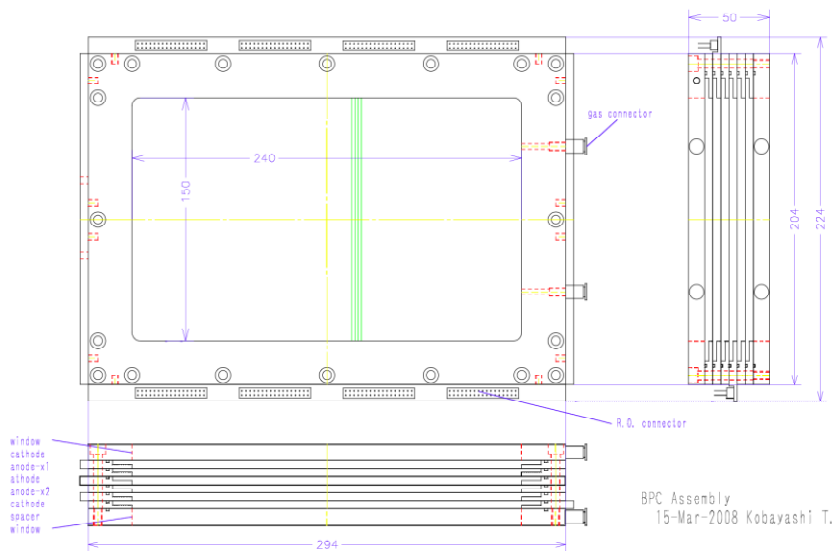
Fig. 2-4-1: BPC assembly

* Status

BPC was built in FY2009 and tested using β rays, p/He/Li beams at 250 MeV/A @200 torr, and Kr beams at 400 MeV/A @20 torr. It has a stable HV plateau with ~100% efficiency even for protons at 250MeV/A. It can be operated above 1 MHz without serious problems.

[2-4-3] Beam Drift Chambers (BDC1, BDC2)

* Design

Two sets of BDC's are used to measure the phase space of the incident secondary beams on the reaction target.　It is a Walenta-type drift chamber with 2.5mm drift distance for high beam rates.　BDC is shown in Fig. 2-4-2, and summarized in the table.

Anode wire	$16 \mu m \phi$ Au-W/Re
Potential wire	$80 \mu m \phi$ Au-Al
anode – potential (drift) distance	2.5mm
anode – cathode gap	2.5mm (combination of 2.4mm & 2.6mm-thick G10)
cathode	8μ m-thick Al-Kapton, x 9
gas window	4μ m-thick Aramid, x2
effective area	80mm x 80mm
anode configuration	xx'yy'xx'yy'
#anode / plane x #planes	16 wires/plane x 8 planes = 128 wires/detector
Operation gas	He+60%CH_4 at 1 atm, i-C_4H_{10} below 200 torr
HV	cathode, potential
Readout / 2sets	ASD x16,　ASD PS x2,　TDC x4
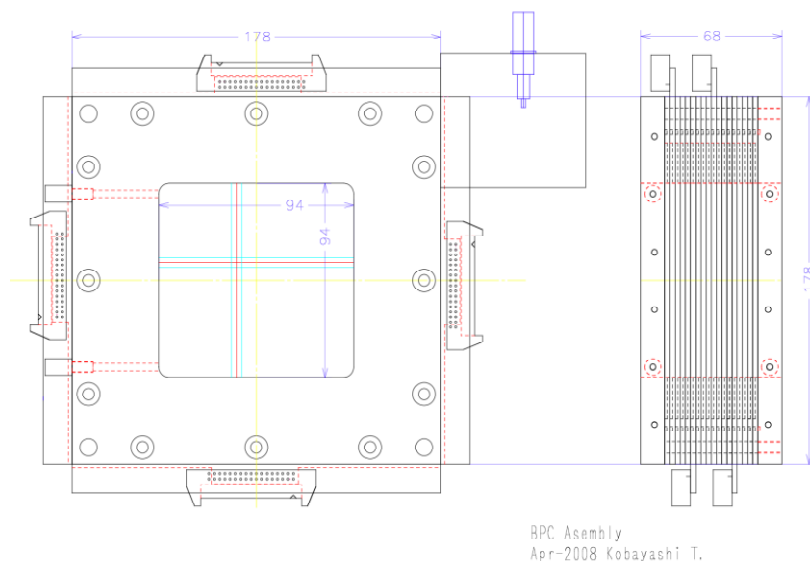
Fig. 2-4-2 : BDC assembly

* Status

2 BDC's were built in FY2009.　Drift chambers of the identical type have been used in experiments at RARF/RIBF/HIMAC for measuring the phase space of protons, He, Li, Be, and C beams between 60 to 300 MeV/A, up to 1MHz, using He+60%CH_4 gas mixture.　Typical position resolution /plane is ~120 μ m (rms). Operation with i-C_4H_{10} at low pressure has been tested.

BDC will be used in the detector box for low-pressure operation (planned to be finished in FY2010).

[2-4-4] <u>F</u>orward <u>D</u>rift Chamber 1 (FDC1)

* Design

   FDC1 is placed between the target and SAMURAL magnet in order to measure the emission angle of the projectile fragments.   It also has wide opening in order not to interfere with projectile-rapidity neutrons at zero degrees.   It is a Walenta-type drift chamber with 5mm drift distance in order to handle relatively high beam intensity right after the target.

anode wire	20 μ m ϕ Au-W/Re
potential wire	80 μ m ϕ Au-Al
anode – potential (drift) distance	5mm
anode – cathode gap	5mm (5mm-thick G10)
cathode	8 μ m-thick Al-Kapton, x 15
gas window	8 μ m-thick Al-Kapton, x2
effective area	315mm ϕ
open area for neutrons	620mm x 340mm
anode configuration	xx'uu'vv'xx'uu'vv'xx', ($\pm 30^\circ$ for u/v)
#anode / plane x #planes	32 wires/plane x 14 planes = 448 wires
operation gas	He+60%CH_4 at 1 atm, i-C_4H_{10} at low pressure
HV	cathode, potential
Readout	ASD x28, ASD PS x3, TDC x7 1 VME crate (with BDC1,2)
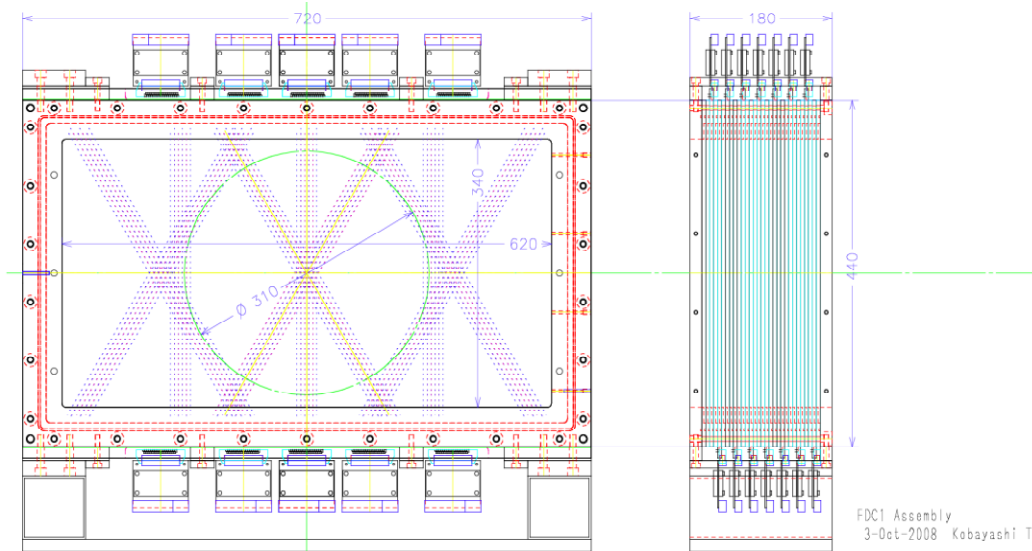
Fig. 2-4-3 : FDC1 assembly

* Status

   FDC1 was built in FY2009.   At the beginning, it had a serious HV leakage due possibly to soldering flux on the G10 boards.   After cleaning the surface and HV conditioning, HV could be set with full

efficiency for beta rays.   It is being tested using cosmic rays.

FDC1 will be used in the detector box for low-pressure operation.   Detector box will be constructed in FY2010.   Connection between target vacuum chamber and also SAMURAI vacuum chamber need to be designed.

[2-4-5]   Forward Drift Chamber 2 (FDC2)

* Design

FDC2 is placed after SAMURAI magnet for rigidity analysis of projectile fragments.   The cell structure is hexagonal with 10mm drift length.   Two staggered planes named super layer, such as xx', are separated by 100mm pitch with shield planes in between.
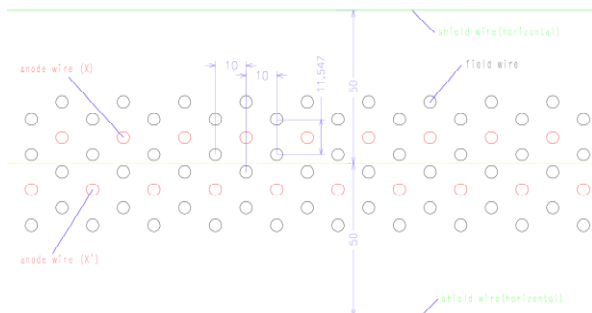
Fig 2-4-4 : FDC2 cell structure

Although it was originally planned to put FDC2 in the detector box for low-pressure operation, FDC2 will be operated at 1 atom for the time being due to technical difficulties.

| Anode wire	$40\,\mu\mathrm{m}\phi$ Au-W/Re, 20mm pitch
Field & shield wire	$80\,\mu\mathrm{m}\phi$ Au-Al, 20mm pitch
Cell structure	hexagonal, 10mm drift length
Configuration	s-xx'-s-uu'-s-vv'-s-xx'-s-uu'-s-vv'-s-xx'-s ($\pm30^{\circ}$ for u/v)
window	2296mm x 836mm
#anode wires (dummy)	224(4) anodes/super layer x 7 super layer = 1568 (28) anodes
#field / shield wires	4788 (field), 328 (shield)
Operating gas	He+60%CH$_4$ at 1 atm (i-C$_4$H$_{10}$ below 100 torr)
HV	field wires, shield wires
Readout	ASD x98, ASD PS x11, TDC x25, 2 VME crates
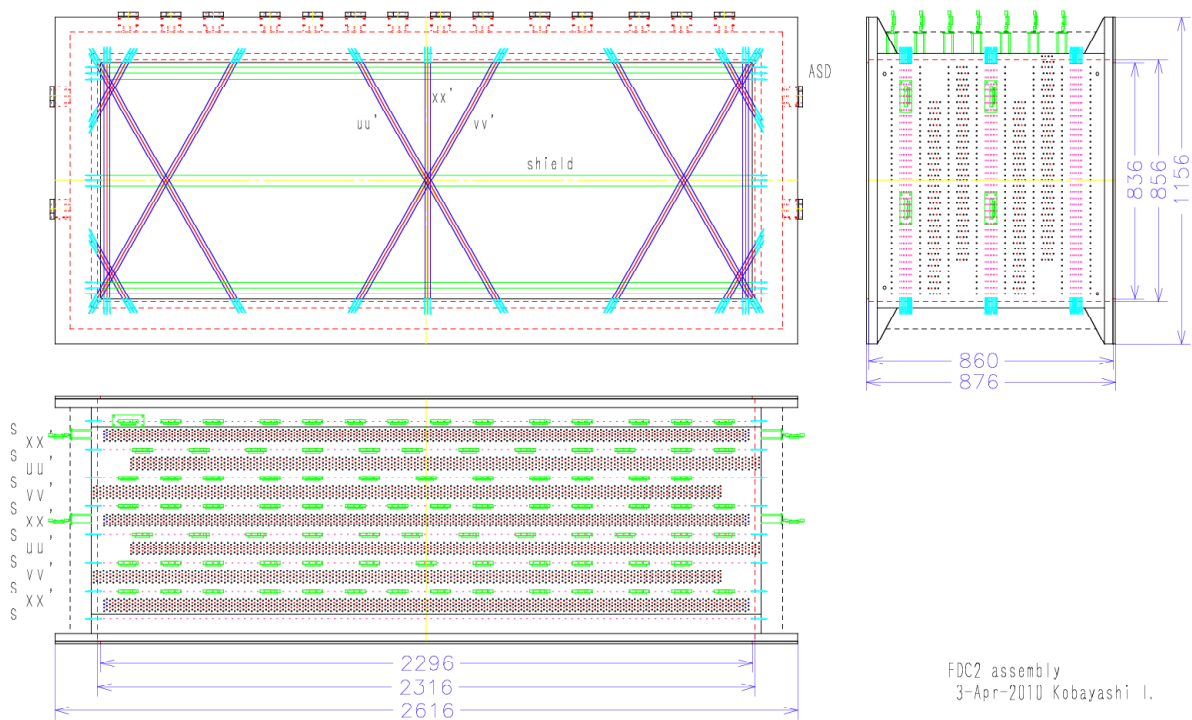
Fig. 2-4-5 : FDC2 Assembly

* Status

FDC2 is under construction. FDC2 itself & detector stand will be finished by the end of FY2010. Tests using β-rays & cosmic rays will be done by the fall of FY2011.

[2-4-6]　Proton Drift Chamber 1, 2 (PDC1, PDC2)

* Design

PDC1 and PDC2 are placed downstream of SAMURAI magnet, and used to measure the momentum of projectile-rapidity protons. Since counting rate is expected to be low and in order to reduce number of planes, position information is obtained using the cathode readout method. For the anode plane, Walenta-type drift chamber, with 8mm drift length, is adopted in order to reduce the number of anode wires. Three kinds of cathode orientation are used to detect multi particles.

Parameters for the cathode readout are as follows.

anode wire	30 μmϕ Au-W/Re, 16mm pitch (8mm drift length)
potential wire	80 μmϕ Au-Al, 16mm pitch
anode – cathode gap	8mm
cathode wire	80 μmϕ Au-Al, 3mm pitch
cathode strip width	12mm (4 cathode wires are or-ed for one strip)

Present design of PDC is as follows. Anode wires are or-ed and positive HV is applied. Anode wires are not readout. Slight negative HV is applied to potential wires. Cathode strips are directly connected to the readout without decoupling capacitors.

Present design of the PDC is shown in Fig 2-4-6.

42

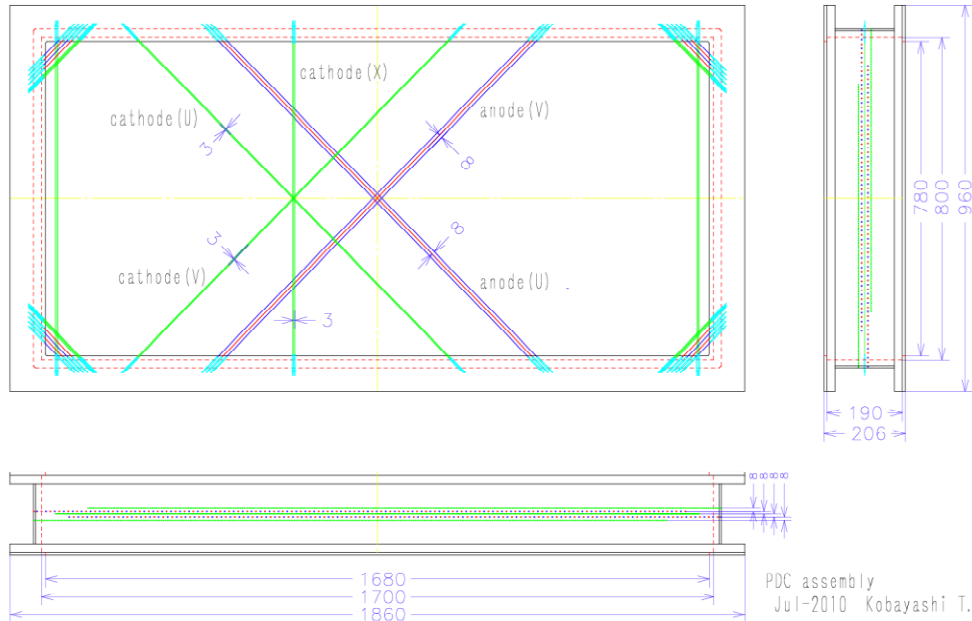| configuration	cathode(U)-Anode(V)-cathode(X)-anode(U)-cathode(V)
wire angle	X(0°), U(+45°), V(-45°)
Effective area	1700mm x 800mm
anode wire (U,V)	106 anodes/plane x 2cplanes = 212 anodes
potential wire (U,V)	107 potentials/plane x 2 planes = 214 potentials
cathode wire (U,V,X)	544 wires/plane, 136 cathode strips (4 wires are or-ed)/plane
HV	Anode(+), potential(-)
Operating gas	Ar+25% i-C_4H_{10} or Ar+50%C_2H_6

Fig 2-4-6: PDC assembly

*Readout (status)

We have tested the charge division readout for cathode signals in order to reduce the readout channel. Cathode strips are daisy-chained by resistors, and cathode charges are read out via charge sensitive pre amp in every 8 strips. Using a prototype detector (600mm x 480mm effective area) with roughly the same geometry, position resolution of 1mm (rms) were obtained for x-rays. With this method, about 110ch of charge sensitive preamp, shaping amp, and peak sensitive ADC's are necessary to read 2 PDC's.

Since 2 proton events can not be handled properly by this method, we are developing a new readout circuit: every cathode signals are connected to charge sensitive preamp, shaper, sample & hold, and digitized in the front-end board (FEB, 16ch/board), and digital data are sent to the VME memory. This method also improve the position resolution by ~factor of 5. About 810 ch of circuits (8-9 FEB's/plane x 6 planes) are necessary.

* Status

Design of PDC is almost finished, and PDC will be constructed by the middle of FY2011. Budget for the new individual readout is not decided yet.

[2-4-7] Ion Chamber for Beam (ICB)

* Design

ICB is a multi-layer ion chamber, and placed upstream of the target.   It is used to measure the charge of incident secondary beams.

| electrodes	12μ m-thick Al-Mylar , 10 anode & 11 cathode planes
Anode-cathode gap	21mm
window	16μ m-thick Aramid
effective area	140mm x 140mm x 420mm (deep)
gas	P10 @1atm
HV	anode(+)
readout	10ch, preamp (Mesytec-MPR16 with 10μ s decay time), shaping amp (MSCF-16LE, active BLR, unipolar output, 0.25μ s shaping time), and peak sensitive ADC (MADC32)
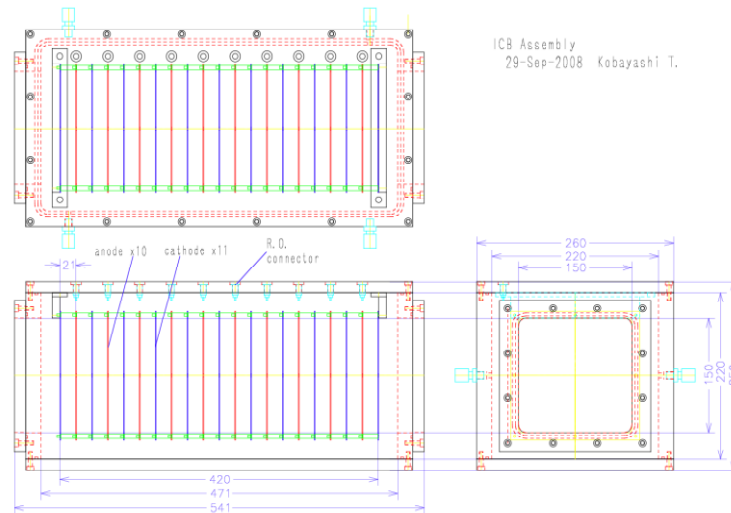
Fig 2-4-7: ICB assembly

* Status

ICB was built in FY2008, and tested using primary & secondary beams from [84]Kr.   Optimum HV and shaping time have been studied.   Pulse height resolution was 0.9% (rms) for [84]Kr at 400MeV/A, corresponding to σ_z=0.17 at z=38.

[2-4-8] Ion Chamber for Fragment   (ICF)

* Design

ICF is a multi layer ion chamber, and placed after the SAMURAI magnet.   It is used to measure the charge of projectile fragments.

Due to several technical difficulties (available size of double-sides Al-Mylar foils, method to make double-sided segmented anodes, etc.), effective area of the present ICF is much smaller than that of FDC2.

We should have used the wire cathode as well to have larger effective area.

electrodes	12 anode & 13 cathode planes
anode-cathode gap	20mm
effective area	750mm (H) x 400mm (V) x 480mm (deep)
anode	80 μ m ϕ Au-Al, 5mm pitch, 18 wires are or-ed to make a 90mm-wide strip, 2 strips are or-ed for readout (4ch/plane)
cathode, window	12 μ m-thick Al-Mylar
Gas	P10 @1atm
HV	cathode (-), anode is at ground potential
readout	4ch/plane x 12 planes = 48ch, preamp (Mesytec-MPR16 x3 with 10 μ s decay time), shaping amp (MSCF-16LE x3, active BLR, unipolar output, 0.25 μ s shaping time), and peak sensitive ADC (MADC32 x2)
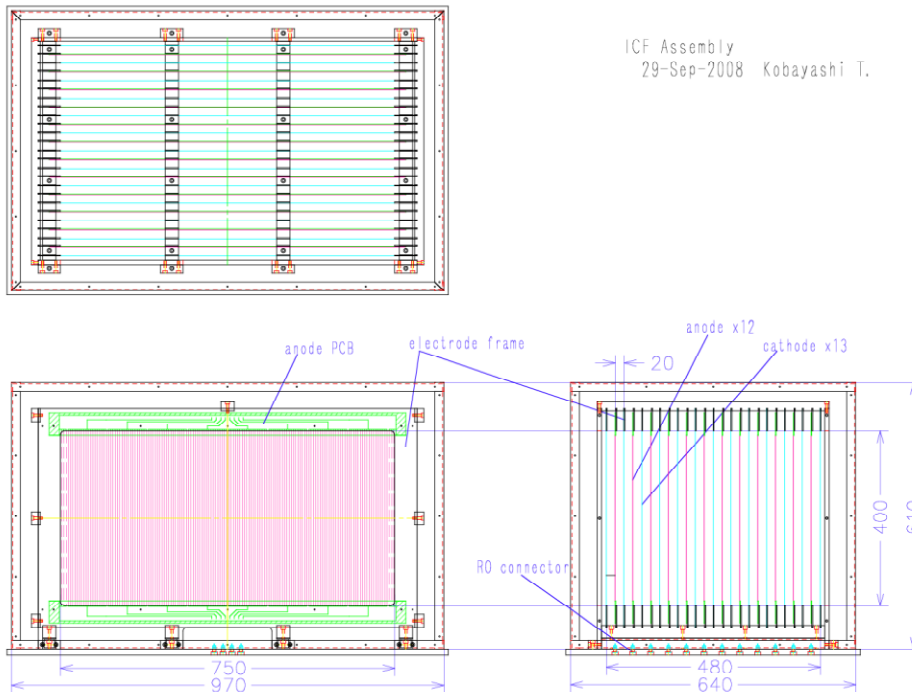
Fig 2-4-8 : ICF assembly

* Status

ICF is under construction, and will be finished in FY2010.   Since the horizontal size of ICF is small compared with the horizontal size of FDC2, detector stand will have a mechanism to move ICF along FDC2.

[2-4-9] Hodoscope for Fragment/Proton (HODF, HODP)

* Design

HODF and HODP are conventional scintillator hodoscopes. They are placed after FDC2 and ICF to measure TOF and charge of particles.

plastic scintillator	BC408, 1200mm(V) x 100mm(H) x 10mm(T)
slat	Plastic is coupled to HPK H7195 PMT (with a booster connector) via 100mm-long fishtail light guide.
Effective area	16 slats/hodoscope, 1600mm(H) x 1200mm(V)
HV	32ch/hodoscope x 2 = 64ch, with additional HV's for booster, CAEN A1733N x6(+4)
Readout	16ch CAMAC discriminator (Phillips 7106) x4, 500nsec logic & analog cable delay x 64, CAEN 32ch ADC V792AC x2 CAEN 32ch TDC V775AC x2
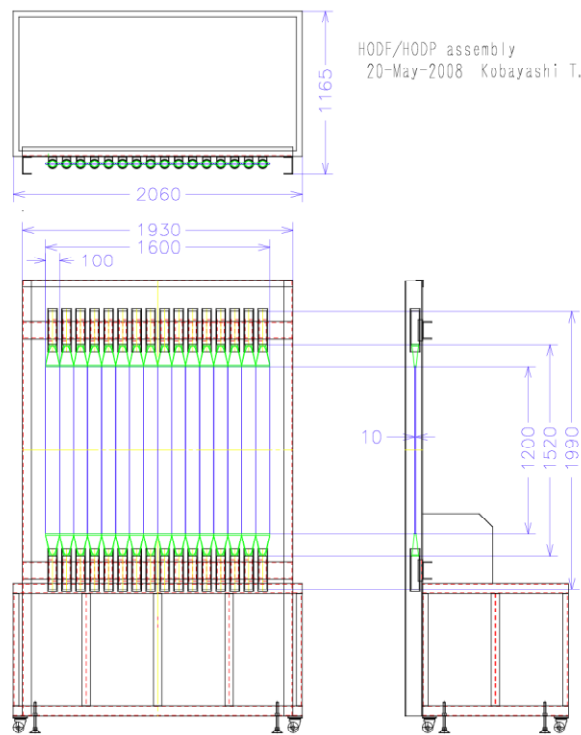
Fig 2-4-9 : HODF/HODP Assembly

*Status

hodoscope slats and detector stands were built.   Since the stands cannot be moved using cranes, hodoscope slats are not yet mounted on the detector stands.   They will be assembled after assembly of the iron blocks for the magnet is finished (summer of FY2011).

[2-4-10]   Total Internal Reflection Cherenkov (TIRC)

* Design

TIRC is a Cherenkov detector operated at the total internal reflection (TIR) threshold.   Since photon numbers increase sharply at the TIR threshold, good velocity resolution is expected.   Refractive index of the radiator chosen is n~1.9 so that the TIR threshold is around 250 MeV/A.

radiator	TAFD30(n~1.92), 65mm x 240mm x 2mm^t (max. size available)
PMT	HPK H6559 (3" ϕ) with booster connector, radiator is viewed by 2 PMT's. 10 PMT's available
effective area	632(317)mm x 240mm(V), covered by 10(5) elements
HV	20(10) ch, CAEN A1733N x2(1)
readout	20(10) x 500nsec cable delay, CAEN 32ch ADC V792AC x1
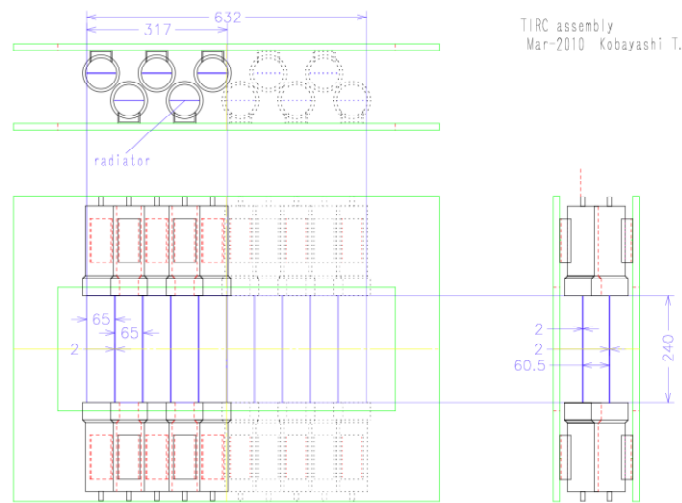
Fig 2-4-10 : TIRC assembly

* Status

We have tested prototypes with radiators of 240 x 65 x 1mm^t and also 2mm^t using energy-degraded Ar & Kr beams between 170 – 400 MeV/A.   From the study on position & angle dependences, we decided to put PMT's on both side of the radiator.   From the energy dependence of the Cherenkov light yield (Fig. 2-4-11a), energy dependence of the velocity resolution is estimated (Fig. 2-4-11b).   Effect of the TIR threshold is clearly seen. Velocity resolution of about 0.2% (rms), which is factor of 2 worse than necessary, was obtained.   We also decided to use 2mm-thick radiators.
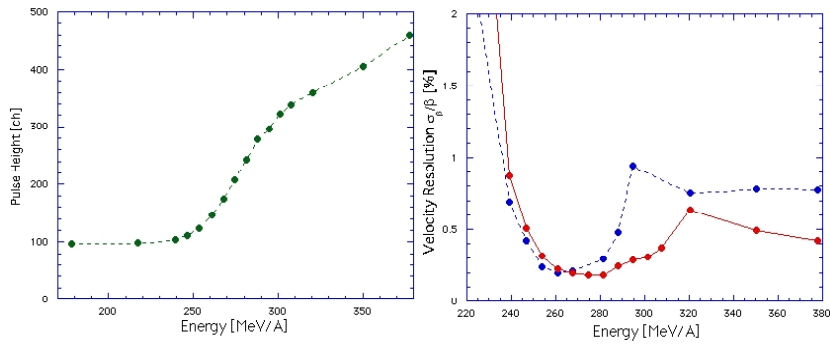
Fig 2-4-11 : Energy dependence of (a) light yield and (b) velocity resolution for Kr beam.

Using rigidity-analyzed ($\Delta p/p \sim 0.1\%$) secondary beams at ~270 MeV/A, we have studied the mass separation. As shown in Fig. 2-4-12, isotopes around mass 70 could be separated with about 4 σ separation for rigidity-analyzed secondary beams ($\Delta p/p \sim 0.1\%$). Due to the thickness of the radiator (~1.2 g/cm^2), reaction loss in the radiator is estimated to be about 5%.
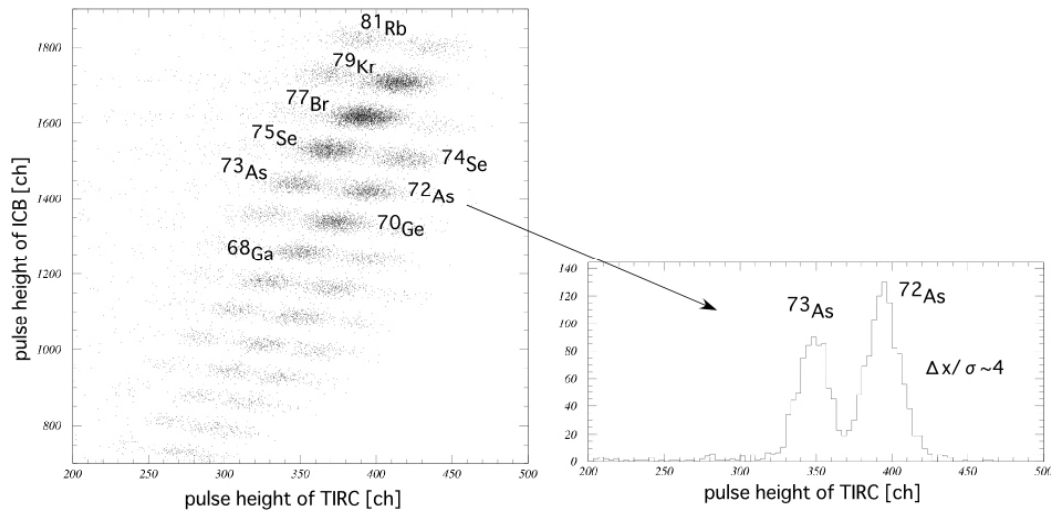

Fig. 2-4-12 : Isotope separation of A~80 region for rigidity-analyzed secondary beams at 270MeV/A

Prototype study shows that TIRC has enough mass resolving power below mass 80 around 270 MeV/A. But we have also noticed the radiation-damage effect.

We have 10 radiators and 10 PMT's available. Using available parts, we can build a TIRC hodoscope with can cover 320mm (H) x 240mm (V) with 5 elements as shown in Fig 2-4-10. Radiators and PMT's will be housed in a detector box which serves as a magnetic and light shield box. Five detector elements will be assembled in FY010, and detector box with stands will be finished by the end of FY2011.

[2-4-11] <u>T</u>otal <u>E</u>nergy <u>D</u>etector (TED)

* Design

crystal	Pure CsI, 100mm x 100mm x 50mm-thick
PMT	HPK – R6233HA(3" ϕ), with non-UV window, booster connector
breeder	tapered, with high breeder current (3mA @1kV),
effective area	800mm(H) x 400mm(V), with 8 x 4 (32) crystals
HV	32 ch, CAEN A1733N x3
readout	32 x 500nsec cable delay, CAEN 32ch ADC V792AC x1

* R&D for TED

As a total energy detector, we have tested (1) NaI(Tl) coupled to PMT, (2) HP-Ge crystal, (3) CsI(Tl) coupled to photodiode, using Ar & Kr & secondary beams between 200 – 400 MeV/A.   Energy resolution of 0.3 – 0.4 % (rms)   for total energy of 25 – 30 GeV was obtained only at low counting rate (below 1kHz).

Since above detectors are relatively slow, we have also tested pure CsI crystal coupled to PMT.   It has smaller light output compared to CsI(Tl), but has faster decay time and believed to be strong against the radiation damage.   After high-current tapered breeder was designed, energy resolution of 0.2 to 0.4% was observed for Kr beams at 400 MeV/A.   By comparing the light output between Ar and Kr beams, large saturation effect was observed.   Since energy resolution between PMT with UV window and with non-UV window has no noticeable difference, PMT with non-UV window was selected.   Light output was stable for beam rates up to 10-20kHz.   It was also observed that the pulse shape for heavy ion is different from those for γ-rays, electrons, and possibly protons.

Although there are many phenomenon which we cannot understand, we studied the isotope separation for rigidity-separated (Δp/p~0.1%) secondary beams at 270 MeV/A.   Configuration of the detector is shown in the table.   Combined with the energy degrader in front of TED,   isotopes around mass 70 region could be separated with ~6σ separation as shown in Fig 2-4-13.   The reaction loss in the degrader and the CsI crystal is estimated to be about 15%.
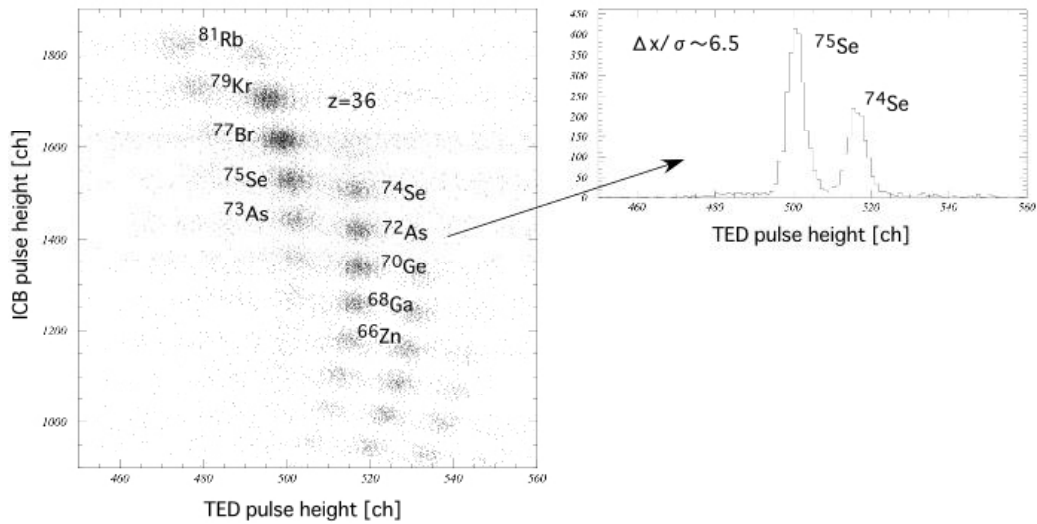
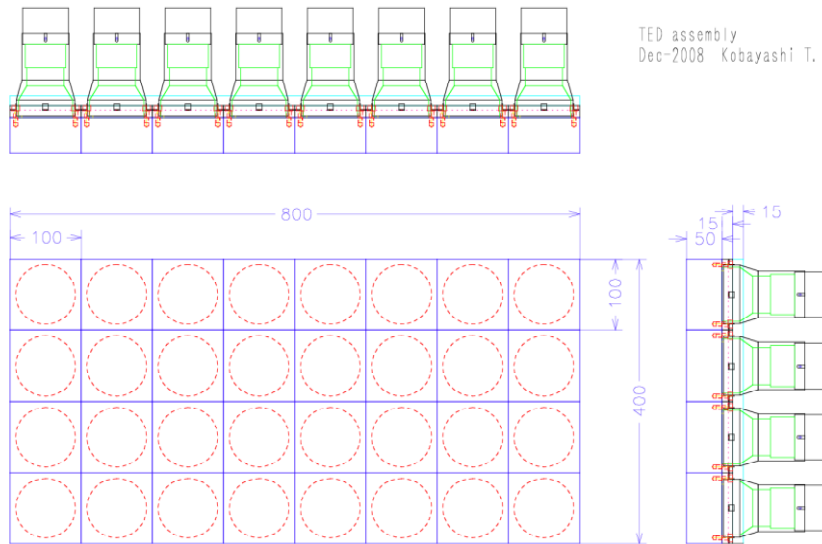Fig 2-4-13 : Isotope separation of A~80 region for rigidity-analyzed secondary beams at 270 MeV/A

Fig 2-4-14 : TED assembly

* Status

32 pure CsI crystals and 32 PMT's are available. Prototype tests showed that this combination has enough mass resolving power for fragments below A~80 at ~270 MeV/A, at least for a short time interval. 32 detector elements will be arranged in 4 x 8 matrix to cover 800mm x 400mm. Whole assembly is placed in the detector box which serves as a light shield and a magnetic shield. Since pure CsI has relatively large temperature dependence of ~1%/deg, temperature of the crystals will be monitored.

32 detector elements will be assembled in FY2010. Detector box and stand will be finished by Mid FY2011.

[2-4-12] Status & Outlook

All the detectors adopted in SAMURAI are, more or less, conventional except TIRC. They are mostly under construction without major problems.

Performance of position detectors will be studied from low-Z region (C, O, Ne where we have experience) towards heavier region (where we have few experience) in 3 steps: z~20, z~28, and z~50.

One of the possible problems is a rate capability. One of the key detectors for experiments in A~100 region are TIRC and TED. In terms of mass resolution, they both have enough velocity or total-energy resolution. However, TIRC seems to have strong radiation damage effect and TED can be stably operated only below ~20kHz.

Since we are in the so-called "beam factory" where high intensity secondary nuclear beams are easily available, detector developments, especially for PID detectors, for high-rate operation are essential in order to fully exploit the capability of the facility.

[2-5] Neutron Detector NEBULA

T. Nakamura*, Y. Kondo, Y. Kawada, T. Sako, R. Tanaka (Tokyo Tech), Y. Satou (Seoul National Univ.)

[2-5-1] Requirements for neutron detection

The neutron detector array NEBULA (**NE**utron Detection System for **B**reakup of **U**nstable Nuclei with **L**arge **A**cceptance) is being constructed as a key element associated with the SAMURAI facility at RIBF, to measure the four momentum vector(s) of fast neutron(s) at about 100-300 MeV emitted in a small cone due to kinematical focusing following a breakup reaction of a neutron-rich projectile. The momentum vector(s) are then used to reconstruct the invariant mass (and E_{rel} and E_x) of the excited system of a projectile, which is of interest. The presumed number of neutrons to be detected ranges from 1 to 4. Required conditions of the NEBULA are summarized as follows.

- Large Acceptance: Large acceptance sufficient for the detection of neutrons emitted in the breakup reactions of neutron-rich unstable nuclei up to the relative energy of 8 MeV ($>\sim50\%$).
- High Detection Efficiency: Intrinsic efficiency should be higher than 60% for $1n$ detection and 20% for $2n$ detection.
- Good relative energy resolution ($\Delta E_{rel}\sim300$ keV at $E_{rel}=1$ MeV, $\Delta E_{rel}\sim1$ MeV at $E_{rel}=10$ MeV) for obtaining a reasonably good energy spectrum with the invariant mass spectroscopy
- Multi-neutron detection capability. The goal is that NEBULA can unambiguously detect 4 neutrons in coincidence with 5% intrinsic efficiency

[2-5-2] Specification

The NEBULA device consists of neutron detectors (NEUT) and charged-particle veto detectors (VETO), whose specifications are summarized in Table 2-5-1 and Table 2-5-2, respectively. The NEUT are funded only half of the original design at the moment (as of Oct.2010), which corresponds to 240 modules of plastic scintillator rods. Each module of NEUT has the size 12(H)$\times$180(V)$\times$12(D) cm^3, each end of which is coupled to PMT via the light guide.

Neutron Detectors (NEUT)		
Geometry of 1 Module	$12(H)\times180(V)\times12(D)$ cm^3 (25.92*liter*, 26.7kg), Rectangular Shape	
Scintillator	BC408 (Saint Gobain)	
Photomultiplier Tube	R7724ASSY, Hamamatsu	
	Full Spec.	Half Spec.(Funded)
Number of Modules per 1 Layer	$30\times2=60$	$30\times2=60$ (or 30)
Number of Layers	4	2 (or 4)
Total Number of Modules	240	120
Number of Phototubes	480	240

Table 2-5-1: Specifications of neutron-detector part of NEBULA. The left column shows the ones for the original full specification, and the right column shows the ones funded at the moment (as of Oct.2010). The funded part corresponds to half the full specification.

Veto Detectors (VETO)	
Geometry of 1 Module	$32(H)\times190(V)\times1(D)$ cm^3 (6.08*liter*,6.3kg), Rectangular Shape
Scintillator	BC408 (Saint Gobain)
Photomultiplier Tube	R7724ASSY, Hamamatsu
Number of Modules per 1 Layer	12
Number of Layers	4
Total Number of Modules	48
Number of Phototubes	96

Table 2-5-2: Specifications of charged-particle veto detectors (VETO) of NEBULA. The VETO is fully funded as originally designed.

[2-5-3] Basic Setup

Hereafter, only the funded part is described unless it is explicitly written. Two possible configurations are presumed for NEBULA setup, 1) 2-Layer Setup and 2) 4-Layer Setup, whose configurations are shown in Fig. 2-5-1.
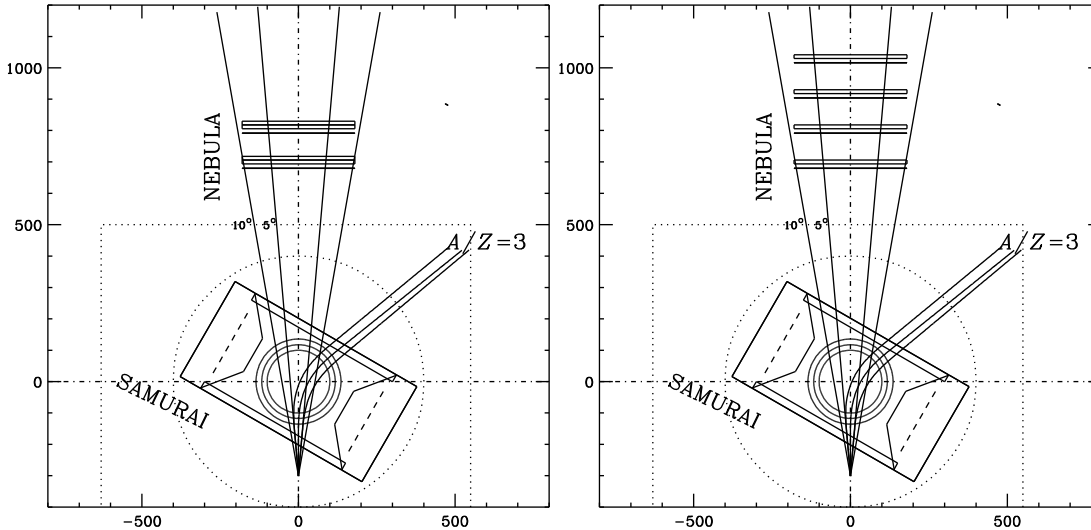

Figure 2-5-1: Left: 2-Layer Setup of NEBULA, which is used for experiments measuring up to two fast neutrons. Right: 4-Layer Setup of NEBULA, which is used for experiments measuring up to four fast neutrons. See text for details.

[2-5-3a] 2-Layer Setup

In this setup, called 2-Layer Setup, the 240 modules of the NEUT is arranged into two layers, located about 1m apart (minimum distance between the rear face of the 1st layer and the front face of the 2nd layer is 610 mm), as shown in Fig. 2-5-1(left). Each layer consists of 30(H)x2(D)(=60 pieces) with a layer of VETO (12 pieces). This is considered to be the primary setup and is used in an experiment measuring 1n and 2n. The intrinsic efficiencies for 1n (ε_{1n}) and for 2n (ε_{2n}) at 250 MeV for the 2-Layer Setup are summarized in Table 2-5-3. The intrinsic detection efficiency for one neutron at 250 MeV as a function of a thickness of BC408 is estimated by the KSUVAX code, as shown in Fig. 2-5-2. One neutron efficiency is estimated to be 40.6% for 48cm thickness (funded part), and 64.1 % for 96 cm thickness for E_{th} (threshold energy) of 5 MeVee (electron equivalent). For 2n detection, the causality analysis may be applied where the velocity detected in the 2nd layer is faster than the one detected in the 1st layer, which will exclude possible cross-talk events due to the scattering of a neutron in the 1st layer. Basically, the same method was successfully applied in the Coulomb breakup of ^{11}Li (T. Nakamura et al., PRL96, 252502, (2006)). Note that this prescription can only be applied for detection of 2n in two different layers, labeled "diff". The efficiency is estimated such that ε_{2n}(diff)= $\varepsilon_{1n}(L1) \times \varepsilon_{1n}(L2)$. For multiple neutron detection, we need to use higher E_{th} of 5 MeVee (electron equivalent) for avoiding γ-ray produced in the detectors. For the detection of 2n in one layer, labeled "same", one may lose efficiency when two neutrons are detected in a very small distance. As in the Coulomb breakup of ^{11}Li (T. Nakamura et al., PRL96, 252502, (2006)), this can be used only after properly evaluating the

efficiency curve. Here, we assume such loss does not happen (corresponding to higher E_{rel}). Here, the efficiency is estimated as $\varepsilon_{2n}(same) = \varepsilon_{1n}(L1)^2 + \varepsilon_{1n}(L2)^2$.

[2-5-3b] 4-Layer Setup

In this setup (4-Layer Setup), the 240 modules of the NEUT is arranged into four layers, which are located about 1m apart with each other (minimum distance between the rear face of the 1st layer and the front face of the 2nd layer is 730 mm)). Each layer consists of 30(H)x1(D)(=30 pieces) with a layer of VETO (12 pieces). The setup is shown in Fig. 2-5-1(right), which is used primarily for experiments requiring $4n$ detection. The intrinsic efficiencies for $4n$ detection (ε_{4n}) is shown in Table 2-5-3. Since 4 neutrons are expected to cause more complicated cross talk, we detect 4 neutrons in 4 different layers with the causality condition being applied. In this case, the $\varepsilon_{4n}(diff) = \varepsilon_{1n}(L1) \cdot \varepsilon_{1n}(L2) \cdot \varepsilon_{1n}(L3) \cdot \varepsilon_{1n}(L4)$. The ε_{4n} value by the funded detectors is 0.011%. If we can obtain the other half of the neutron detectors, the $4n$ efficiency considerably improves to be 0.056%.
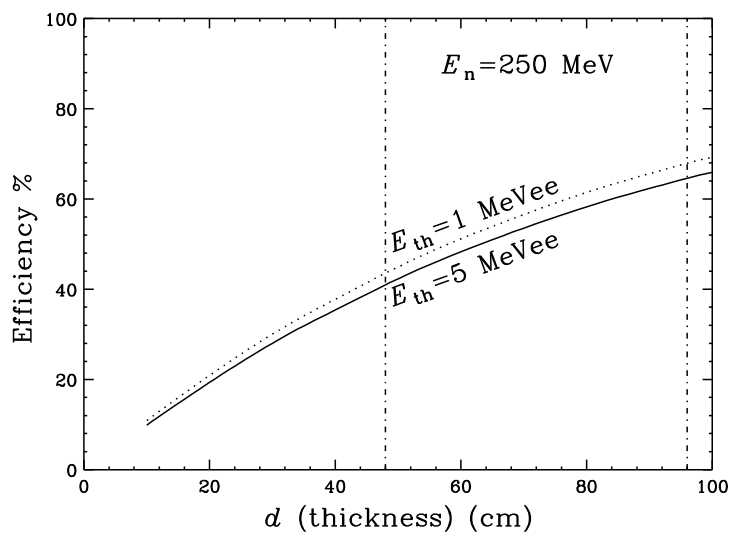

Figure 2-5-2: Intrinsic detection efficiency for one neutron at 250 MeV, estimated by KSUVAX code. The dotted (solid) curve represents the efficiency for the energy threshold of 1 (5) MeVee (electron equivalent). The dot-dashed vertical lines correspond to the thickness of 48 cm (funded), and of 96 cm (designed thickness).

	ε_{1n}(%)	ε_{2n}(%)(sum,same,diff)			ε_{4n}(%)(4-layer diff)
24cm×2layer	41.0	12.6	8.5	4.1	
12cm×4layer	41.0	10.5	4.3	6.3	0.011
24cm×4layer	64.6	26.6	11.4	15.2	0.056

Table 2-5-3: Summary of $1n$, $2n$, and $4n$ intrinsic efficiencies (ε_{1n}, ε_{2n}, ε_{4n}, respectively) for the NEBULA with 48 cm thickness (funded part), and those with 96 cm thickness (designed). The label 'diff' represents $2n$ events detected with different two layers with the kinematical causality condition being applied, while the label 'same' represents $2n$ events detected with one layer. The 'sum' is the sum of 'same' and 'diff' events.

For 4*n* detection, events detected with 4 different layers with kinematical causality condition cut are considered. downstream of the target position, close to the first layer of the typical 2-Layer setup shown in Fig. 2-5-1.

[2-5-4] Acceptance

Typical acceptance curve as a function of E_{rel} is estimated for the breakup, $^{A}Z \rightarrow ^{(A-1)}Z + n$, as shown in Fig. 2-5-3. Here, the vertical angular coverage of $-5^{\text{o}} < \theta_{V} < +5^{\text{o}}$ and $-10^{\text{o}} < \theta_{H} < +10^{\text{o}}$ is used, which corresponds to neutron detector with an area of 3.6m(H) $\times$ 1.8m(V) located at 10.3 m.

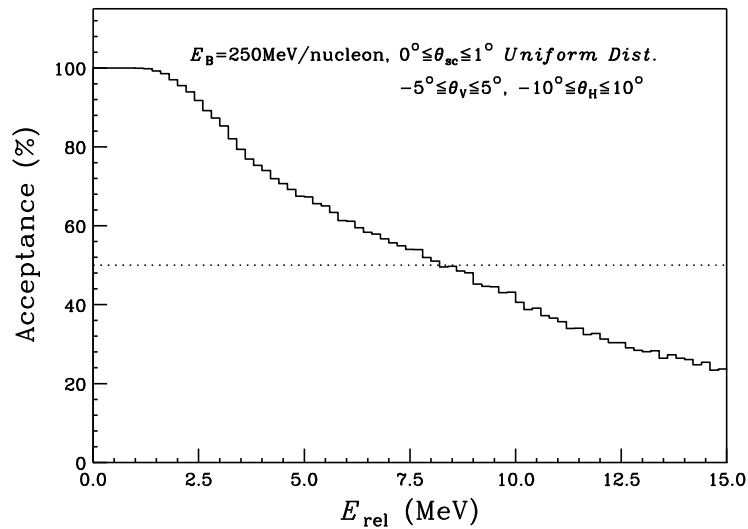Figure 2-5-3: Acceptance is shown as a function of E_{rel} with the vertical angular coverage of $-5^{\text{o}} < \theta_{V} < +5^{\text{o}}$ and the horizontal angular coverage of $-10^{\text{o}} < \theta_{H} < +10^{\text{o}}$. This coverage is realized to set the flight length from the target to be 10.3 m or less.

[2-5-5] Resolution

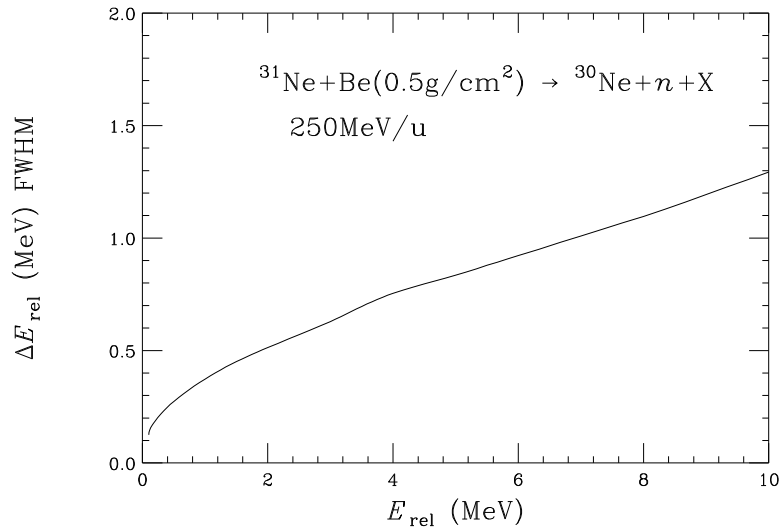Typical relative energy resolution ΔE_{rel} (FWHM) is shown in Fig. 2-5-4 as a function of E_{rel}.

Figure 2-5-4: Typical relative energy resolution ΔE_{rel} (FWHM) as a function of E_{rel}.

[2-5-6] Electronics

Figure 2-5-5 shows the electronic circuit for signals of NEBULA. VME modules (discriminator, TDC, ADC) are controlled by using the crate controller, SBS Model 618-3. The CAEN SY1527LC system with A1535SN boards is used to supply the high voltages of the PMTs.
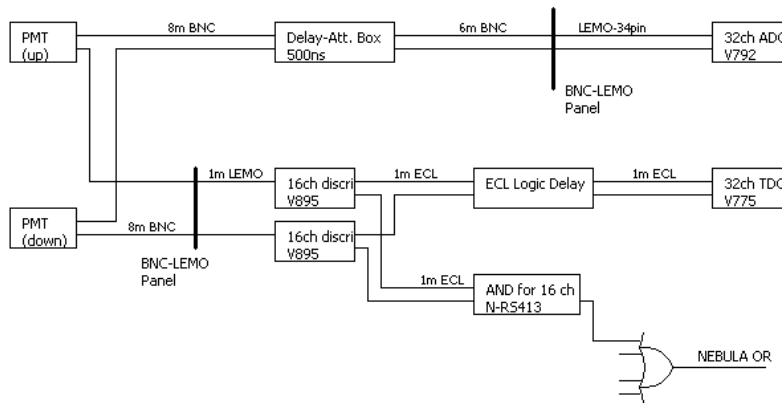

Figure 2-5-5: Electronic circuits for the signals of NEBULA.

[2-5-7] Current Status and future plan

Current status of NEBULA is as follows.

- Fabrication of scintillators, PMTs, and light guides has almost been completed.
  - 3 scintillator rods for NEUT had a problem. They have been exchanged to new ones and will be delivered after fabrication.
  - Signals from PMTs and light leakages have been checked for all the fabricated modules.
- 4 detector frames for setting up the detectors have already been made. Each detector frame has the capability of mounting neutron counters up to 60 modules and a layer of VETO in front of the NEUT layer. Whole of the frame can be moved by using a crane without dismounting the detectors, cables, and electronics.
- Existing detectors have already been mounted to the two detector frames for the 2-Layer configuration experiment.
- A part of cables and electronics have been manufactured.
- The detectors are being tested by measuring cosmic rays.

The schedule plan of NEBULA is shown in Table. 2-5-4.

~Dec. 2010	Detector test of the 1st. Layer by cosmic rays
~Apr. 2011	Connecting cables of the 2nd. Layer
~Jul. 2011	Test of the 2nd. Layer by cosmic rays
Oct. 2011	Test of a part of detectors using high energy neutrons at HIMAC
Mar. 2012	Comissioning & Day-1 experiment of SAMURAI

Table 2-5-4: Schedule of NEBULA

[2-6] Detector System for Proton Breakup Reactions

K. Yoneda*, Y. Togano, M. Kurokawa, A. Taketani, H. Murakami, T. Motobayashi (RIKEN),

K. Kurita (Rikkyo), T. Kobayashi (Tohoku), L. Trache (Texas A&M) and the TWL collaboration

[2-6-1] Requirements for proton breakup reactions

We propose here studies of the proton unbound states in the proton-rich region. The RIBF project will provide a good access to a variety of proton-rich nuclei which so far cannot be studied experimentally. In order to examine nuclear structure of nuclei close to, or beyond, the proton drip line, measurements of the location of the unbound states are critical. In particular, studies of proton unbound states are important for astrophysical interest, since energy and width of such states influence radiative capture cross sections under astrophysical conditions, and hence play an important role in exploring nucleosynthesis processes.

Such unbound states are identified with the invariant mass method, through the measurement of the kinetic energies and scattering angles of breakup products. For two body breakup reactions, the relative energy resolution is calculated as,

$$\delta E_{rel} = \delta M_{inv} = \sqrt{\left(\frac{\partial M_{inv}}{\partial \theta_{open}}\right)^2 \delta\theta_{open}^2 + \left(\frac{\partial M_{inv}}{\partial P_1/P_1}\right)^2\left(\frac{\delta P_1}{P_1}\right)^2 + \left(\frac{\partial M_{inv}}{\partial P_2/P_2}\right)^2\left(\frac{\delta P_2}{P_2}\right)^2} \ .$$

The condition of $E_{rel} = 1$ MeV and $E_{in} = 250$ AMeV and $\mu \sim m_p$ leads to $\dfrac{\partial M_{inv}}{\partial \theta_{open}} < \mathbf{34.1 keV/mrad}$ and

$\dfrac{\partial M_{inv}}{\partial P/P} < 130\,\text{keV}/\%$. For low-lying resonance studies, 0.1 MeV (1σ) resolution at $E_{rel} = 1$ MeV is necessary to separate states experimentally. In order to obtain 0.2 MeV resolution at $E_{rel} = 1$ MeV, the opening angle resolution of 2 mrad and momentum resolution of $\sigma_P/P = 0.8\%$ are required. The momentum resolution required for the mass identification is severer; $\sigma_P/P = 0.2\%$ is required for 5σ separation at $A=100$ region. This momentum resolution is satisfied by the design goal of the rigidity resolution of the SAMURAI spectrometer, 1/700.

[2-6-2] Two Detector Configurations – High Resolution Mode and Large Acceptance Mode

We propose two experimental setups for HI-proton coincidence measurements. One is the high resolution mode, in which proton-rich reaction residues around A/Z~2 are bent in the SAMURAI magnet as much as possible, so that a good momentum resolution is achieved. The other setup is the large acceptance mode, where the resolution is relatively poor but larger acceptance if afforded. In the following, these two modes are described.
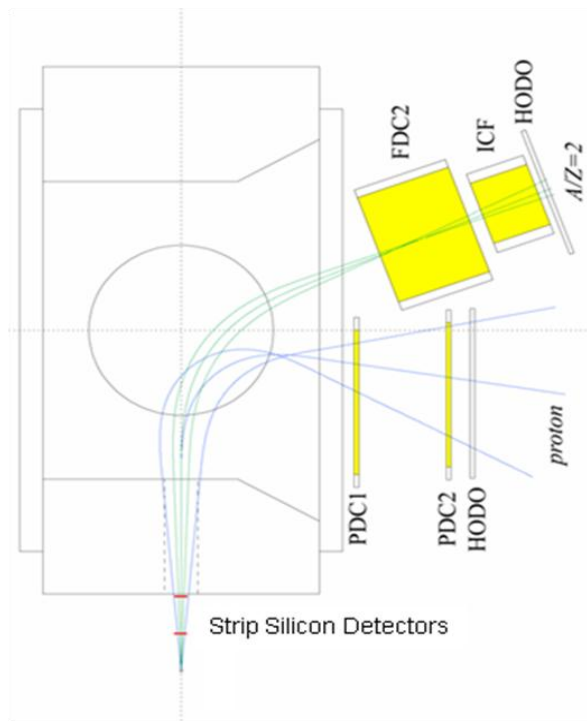
Fig 2-6-1: Detector Configuration for High Resolution Mode

High Resolution Mode

Figure 2-6-1 shows a schematic view of the experimental setup for the high resolution mode. The particle trajectories are drawn for a 3T magnetic field. The reaction products go through a hole for the large bending angles. The resolution attained in this mode for HI is estimated to about 1/700. The hole size is 40cm x 40cm, which covers up to the relative energy of about 4 MeV for the proton breakup at the beam energy of 250 AMeV.

Heavy fragments are bent by in the magnet about 60 degrees, are tracked by the drift chamber FDC2, and are identified by the ToF-ΔE measurement (additionally total E measurement if required).These detectors are described in Section 2-4. Protons are also bent and are tracked by the drift chambers PDC1 and PDC2. Descriptions of PDC1 and PDC2 are given in Section 2-4-6. ToF of the protons are measured by the plastic hodoscope HODO, which is explained in Section 2-4-9.

In order to achieve the opening angle resolution of 2 mrad, silicon microstrip detectors are placed between the target and magnet to measure scattering angles of protons and heavy ions right after the target. One may consider a gas detector, such as a drift chamber for this purpose, but the operation of such a detector is impossible under the condition that the detector is hit by both heavy and light particles; if the high voltage is adjusted for protons, the detector is not operable when heavy particles hit the detector.

As silicon microstrip detectors for this purpose, we adopted GLAST silicon detectors. Two sets of three detectors (in the horizontal, vertical, and diagonal directions) with a thickness of 0.32 mm and an active area of 87mm x 87mm, are located at 50 and 80 cm downstream of the target. The pitch size is 0.228mm. At the beginning we plan to use the detector with three strips bundled into one channel. In this condition, the relative energy resolution attained is estimated to be about 100 keV for the breakup reaction at the beam energy of 250 AMeV.
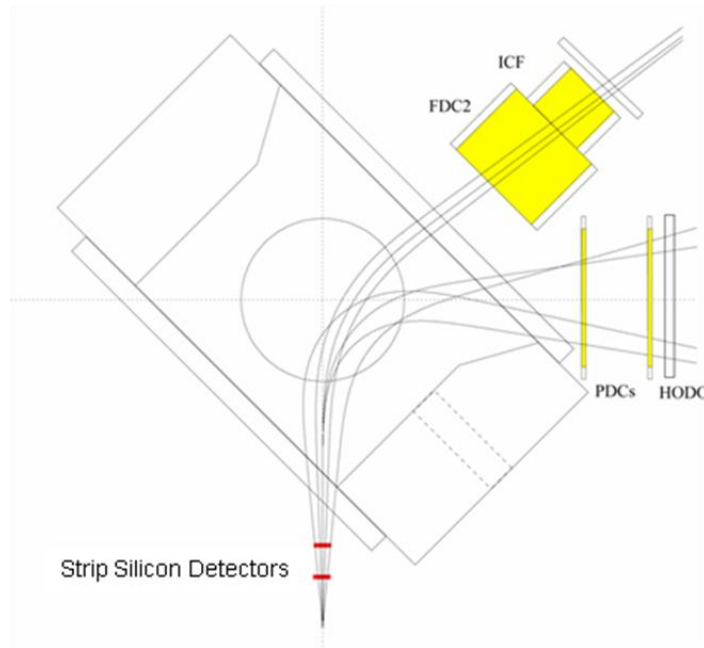
Fig: 2-6-2: Detector Configuration for Large Acceptance Mode

Large acceptance mode

We plan to use another setup configuration shown in Fig. 2-6-2. In this setup, the reaction products are injected to the magnet at 45 degrees with respect to the direction of the magnet yokes. This setup affords larger acceptance especially for light particles, and hence covers the relative energy up to about 10 MeV. This configuration also allows neutron detection at forward angles, which is useful when exclusive measurements for multi particles are required. The rigidity resolution is estimated to be about 1/500. With this resolution we expect to perform breakup measurements up to A~60, but for heavier mass region the high resolution mode may be required.

The detector lineup is almost the same as the high resolution mode. The angles of the protons and reaction residues are measured by two stacks of silicon telescopes which are apart by 300 mm. Reaction residues are also detected after the magnet by a drift chamber for track measurement, an ion chamber for energy loss measurement, and a plastic scintillator wall for TOF measurement. Protons are detected by a drift chamber and a plastic scintillator wall for track and TOF measurements, respectively.

[2-6-3] Current Status of Silicon Strip Detector

Here we report on the current status of the silicon strip detectors we plan to use between the target and magnet. The resolution of the relative energy in the invariant mass measurement is mostly governed by the precision of the angular measurement of light particle, i.e. proton angular resolution in the case of proton breakup measurement. Therefore we measure protons between the target and magnet so that we can surely determine the proton emission angles.

As the position detector, we use the GLAST type silicon strip detector. Geometrical information of the GLAST silicon detector is given above. Two sets of three detectors for vertical, horizontal, and diagonal

position determination, are placed with the distance of 30cm, are placed at 50cm downstream of the target. In this situation, the relative energy resolution is about 100 keV for 1MeV relative energy.

As of October 2010, ten silicon sensors are already available. The detectors are going to be ready after the detectors are connected with an electric board by wire bonding. In order to make the detectors ready for experiments, we have to overcome two difficulties: 1. High density signal processing to deal with signals of about 1500 channels, 2. Large dynamic range to accept signals of both heavy ion and proton which hit a detector in one event.

The first difficulty is overcome by using the HINP16 electronics. HINP16 is the 16 channel integrated circuit which was developed in Washington University in St. Louis. This circuit can process 16 channels in parallel in one chip, and for each channel a shaped signal for ADC and a discriminated signal for TDC are produced (Fig.2-6-3). The circuits are introduced in the collaboration supported by the US DOE Funding, In collaboration with Prof. L. Trache in Texas A&M University and the TWL collaboration (Texas A&M University, Washington University in St. Louis, and Louisiana State University).
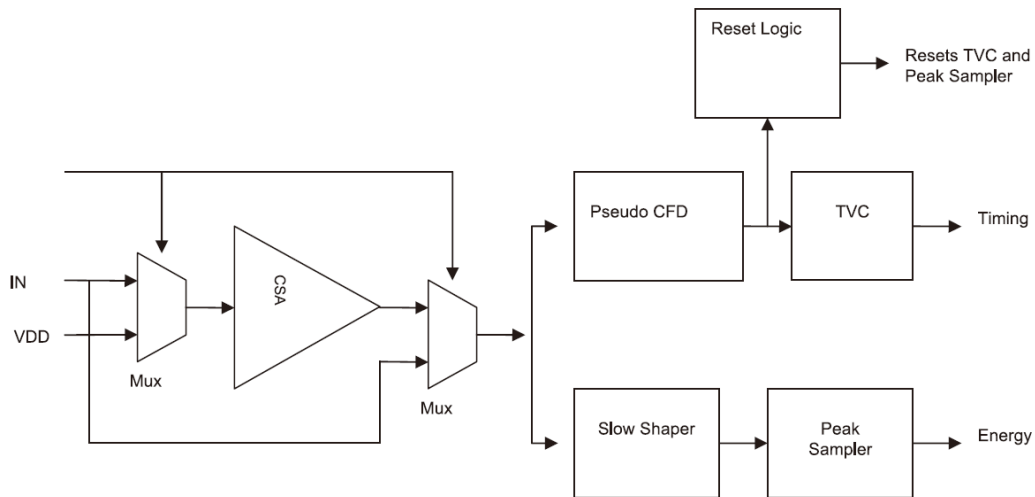

Fig. 2-6-3: Block Diagram of the single channel in the HINP16 Circuit.
Each of 16 channels of the HINP16 consists of a CSA, followed by
a timing and energy branch (G.L Engel et al., NIM A573 (2007) 418).

In order to deal with the second difficulty, we will introduce two things. The first thing is signal split circuits before the preamplifier (Fig. 2-6-4). A signal from each detector strip is divided to the high-gain circuit for proton signal, and low-gain circuit for heavy ion signal. In this circuit, we have to put an additional circuit to deal with the signal saturation; when HI hits the strip, the high gain circuit is saturated, and the saturation ruins behavior of the other low-gain circuit. In order to cope with this problem, we put a saturation suppression circuit on the high-gain amplifier, which provides an escape path of the charge when too much charge comes to the amplifier. This circuit has already been realized on an ASIC for test, and has been confirmed to work as expected. We plan to proceed to the ASIC production phase in FY2011.
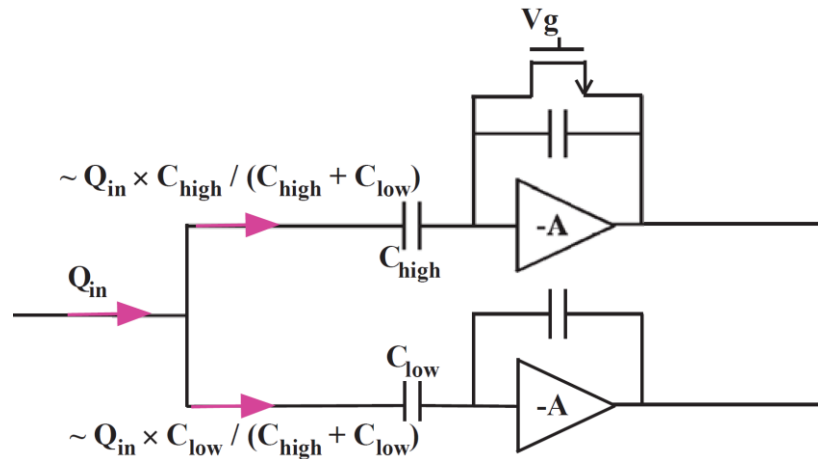
Fig. 2-6-4: Diagram of the signal split circuit. Charge from a detector is divided
to C_{high} and C_{low}, and is amplified independently by high gain and low gain.
In order to prevent saturation in the high gain amplifier, a gate is placed in parallel,
which provides an escape path of charge when too much charge comes into C_{high}.

The second thing we plan to do is to develop a new preamplifier circuit, which has a large dynamic range with low noise, covering about input signal dynamic range typically from 150 keV to 1 GeV, and is coupled to a circuit of non-linear signal response so that the output signal is acceptable for following circuits. The size is compact, accommodating 32 channels in 40mm x 40mm x 50mm. At present the circuit is in the phase of conceptual designing, and we expect to obtain the first trial circuit in FY2011, and to start production in FY2012 if the trial circuit is satisfactory. The merit of this preamplifier is that we do not have to split signals, and hence the total channel number becomes half. Furthermore, this low-noize large dynamic range preamplifier is expected to be useful for many other experiments requiring heavy ion detection.

[2-6-4] Schedule Plan

Our current schedule plan is as follows:
- In FY2010, wire bonding is made on the silicon strip, and signals from the strips becomes visible from the circuit board
- In FY2011, both HINP circuit and signal split circuit starts working with the detector. Overall system test with beam will be performed if possible (at RIBF or at Texas A&M University).
- In FY2012, on-site preparation for RIBF experiments will be made including scattering chambers, DAQs at RIKEN. New preamplifier circuits becomes ready when things proceed smoothly.
- Early in 2013, everything becomes ready for RIBF experiments.

This project is supported by the US DOE Funding, and Grant-in-Aid for Scientific Research (B) in Japan.

[2-7] Detector System for Polarized-Deutron-Induced Reactions

K. Sekiguchi*, T. Kobayashi, Y. Matsuda, graduate students (Tohoku)

High resolution mode of the SAMURAI – Q3D mode-

In experiments where high momentum resolution of $p/\delta p > 1000$ is required, the triplet Q-magnets of the beam line STQ25 is used as analyzer magnets in conjunction with the SAMURAI dipole magnet (the SAMURAI Q3D mode). Schematic view of the experimental arrangement is shown in Fig.2-7-1.
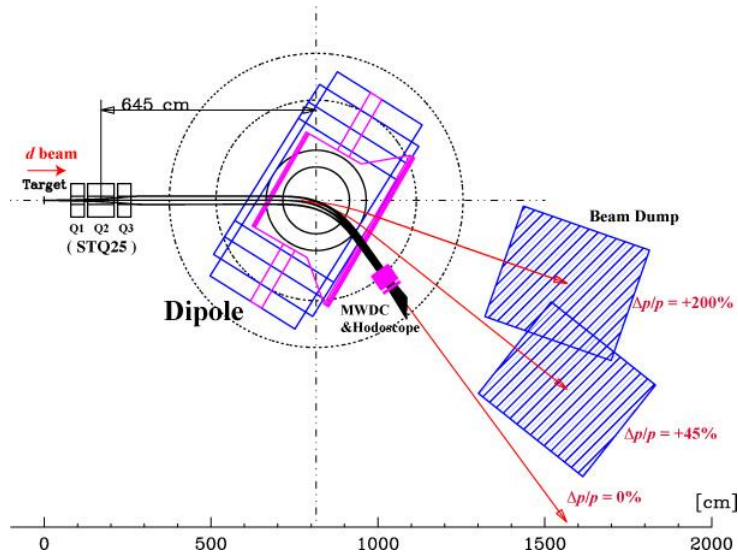

Fig.2-7-1: Schematic view of the experimental setup of the SAMURAI Q3D mode.

The target is installed 815cm upstream from the center of the dipole magnet. The distance between the Q2 magnet of STQ25 and the center of the dipole magnet is 645 cm. The focal plane detectors are located 3 m downstream from the center of the dipole magnet. The expected focal plane detectors are a multi-wire drift chamber (MWDC) and plastic scintillator hodoscope which covers momentum acceptance $\Delta p/p = \pm\ 3\%$. Expected performances of the Q3D mode are,

Dispersion	2.2 m ,
Magnification	$(x\vert x) = 0.43,\quad (y\vert y) = -14.2,$
Vertical angular acceptance	$+/-90$mrad
Horizontal angular acceptance	$+/-20$mrad
$p/\delta p$	$\sim\ 3000$.

The calculations were performed using the OPTRACE code with a realistically calculated magnetic field of the dipole magnet.

Beam dump of deuteron beam

In order to keep good momentum resolution the focal plane detectors are fixed to the ground, and then the magnetic field strength is adjusted depending of the momentum region of interest for the detected particles. Therefore the beam dump which is used for charge collection of the beam is set in an appropriate position depending on the momentum ratio $P(d$ beam$)/(P$(detected particle)/Q). Schematic view of the beam

dump is shown in Fig. 2-7-2. The beam dump is set 6m downstream from the center of the dipole magnet. Charge collection of the beam is performed by a Faraday cup which consists of a lead cylinder with embedded tungsten rod. The lead cylinder is $25cm^{\phi} \times 40cm^{t}$ in size and the tungsten rod is $3cm^{\phi} \times 20cm^{t}$ in size. In order to reduce the emitted neutrons coming from deuteron breakup the Faraday cup is shielded with concrete blocks. The total volume of the concrete blocks are 49 m^3 ($4.0m^{D} \times 3.5m^{W} \times 3.5m^{H}$) and the weight is 120 ton in total. Expected drive of the beam dump is a set of air bearing which moves a heavy load with air power. The open geometry of the SAMURAI makes it possible to place and move such a large size of the Faraday cup assembly.
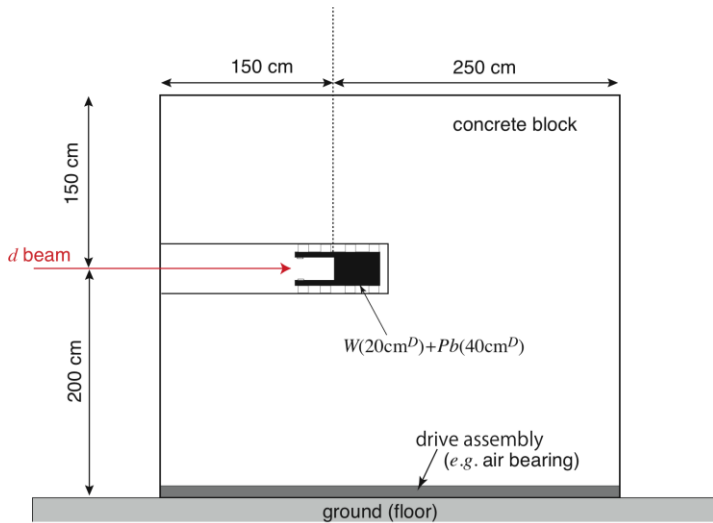

Fig.2-7-2
Schematic view of the beam dump.

Other equipments

In order to perform the experiments the following equipments should also be constructed.

a. Scattering chamber and target system for the SAMURAI Q3D mode

b. Beam monitoring devices for light ions (Z=1) at Big RIPS

c. Exit vacuum window of the SAMURAI dipole magnet

Current status

So far the equipments for the experiments with polarized deuteron beams at the SAMURAI are scarcely funded. The equipments and their costs are listed in the order of priority.

1. Beam dump (50 M JYen),

2. Scattering chamber and target system at SAMURAI in Q3D mode (5 M JYen),

3. Exit vacuum window (3 M JYen),

4. Beam monitoring devices for light ions (Z=1) at Big RIPS (3 M JYen),

5. Focal plane detectors (16 M JYen)

It should be noted that we performed the first experiment with polarized deuteron beams at 250 MeV/nucleon at RIBF and successfully obtained highly polarized deuteron beams in 2009.

[2-8] SAMURAI TPC

T. Murakami* (Kyoto), T. Isobe, A. Taketani, S. Nishimura, Y.Nakai, H. Sakurai (RIKEN),

W.G. Lynch (Michigan State) and SAMURAI TPC collaboration

Summary and Current Status

Since the initial construction budget approved for the SAMURAI project could not cover all detector systems we originally proposed, we formed a "SAMURAI TPC international collaboration" consisted of researchers from USA, UK, France, Italy, China, Germany and Japan and submitted a budget request of $1.2M to the US DOE in December 2008 in order to construct a Time Projection Chamber (TPC) used in the gap of the SAMURAI dipole magnet.

The collaboration also submitted a construction proposal, "Constraining the symmetry energy at Supra-saturation Densities" to the NP-PAC-05 at RIBF in 2009. In the proposal we presented our intention to build a TPC at the National Superconducting Cyclotron Laboratory (NSCL), Michigan State University, USA, using the DOE budget then transport the TPC to RIKEN for symmetry energy experiments at RIBF facility. The RIKEN RIBF could provide an excellent opportunity to explore the density dependence of the symmetry energy at supra-saturation densities ($\rho \approx 2\rho_0$) via pion production with very neutron-rich and neutron-deficient rare isotope beams. The energies that will be available at the RIBF facility allow one to probe densities of about $\rho \approx 2\rho_0$; the range of available beam asymmetries will be wider than what is available at other existing facility in the world and will not be exceeded for next several years. With the SAMURAI TPC, we hope to obtain important constraints on the Equation of State (EoS) by measuring not only the π^+/π^- yield ratio but also light charged particles such as proton, tritons and ^{3}He in intermediate energy heavy-ion collisions.

We plan to combine observables from both pion and neutron-proton data. We will use these data to disentangle the symmetry energy effects from those of neutron-proton effective masses and isospin dependent in-medium cross sections and obtain independent constraints on all three quantities. Using the TPC we envision to measure excitation function for of pion production in ^{132}Sn+^{124}Sn, ^{105}Sn+^{112}Sn, ^{52}Ca+^{40}Ca and ^{36}Ca+^{40}Ca collisions at E/A = 200-300 MeV as well as in stable ^{124}Sn+^{124}Sn and ^{112}Sn +^{112}Sn collisions at E/A = 350 MeV. When the TPC is coupled with a highly efficient neutron detector, such as the NEBULA array at RIKEN, it will be possible to measure neutron-proton spectral double ratios which can also provide significant constraints on the density dependence of the symmetry energy, the neutron-proton effective mass splitting and the isospin dependence of the in-medium nucleon-nucleon cross sections at supra-saturation density. We foresee such a coupled operation will be possible once the TPC becomes ready. Our proposal has been reviewed and strongly supported by the NP-PAC.

For more information on SAMURAI TPC, please refer to the construction proposal "Constraining the symmetry energy at Supra-saturation Densities" submitted by the SAMURAI TPC collaboration in 2009.

[2-9] Summary of the Construction Schedule

   In Table 2-9-1, summary of the construction schedule of the magnets and detectors is shown. In order to be in good accordance with the policy given in the introduction, all the experimental setup required for the coincidence measurement of light HI (Z<20) and neutron will be ready in early 2012. The operation for heavier beams will be studied step by step toward the heavier region, first up to Z~30, and then Z~50. The setup for proton detection will be prepared in 2012. The experimental devices for missing-mass type experiment, polarized deuteron induced experiment, and EOS-TPC experiment will be prepared accordingly.

Table 2-9-1: Summary of Construction Schedule

	2010	2011				2012				2013				2014	
	Q4	Q1	Q2	Q3	Q4	Q1	Q2	Q3	Q4	Q1	Q2	Q3	Q4	Q1	Q2
Dipole magnet															
STQ															
Vacuum system															
HEAVY ION DETECTOR															
BPC, BDC															
FDC1															
FDC2															
ICB															
ICF															
HODO															
TED															
TIRC															
NEUTRON DETECTOR															
NEBULA															
PROTON DETECTOR															
PDC															
Strip silicon															
pol–d setup															
TPC															

[2-10] Experimental Setup in Early 2012

   Planned experimental setup in early 2012 is described in this section, assuming that the "Day-One" experiments are (γ,n)-type Coulomb breakup experiments in C, O, and Ne region followed by other experiments in Ni region.   The proposed setup is shown in Fig. 2-10-1.
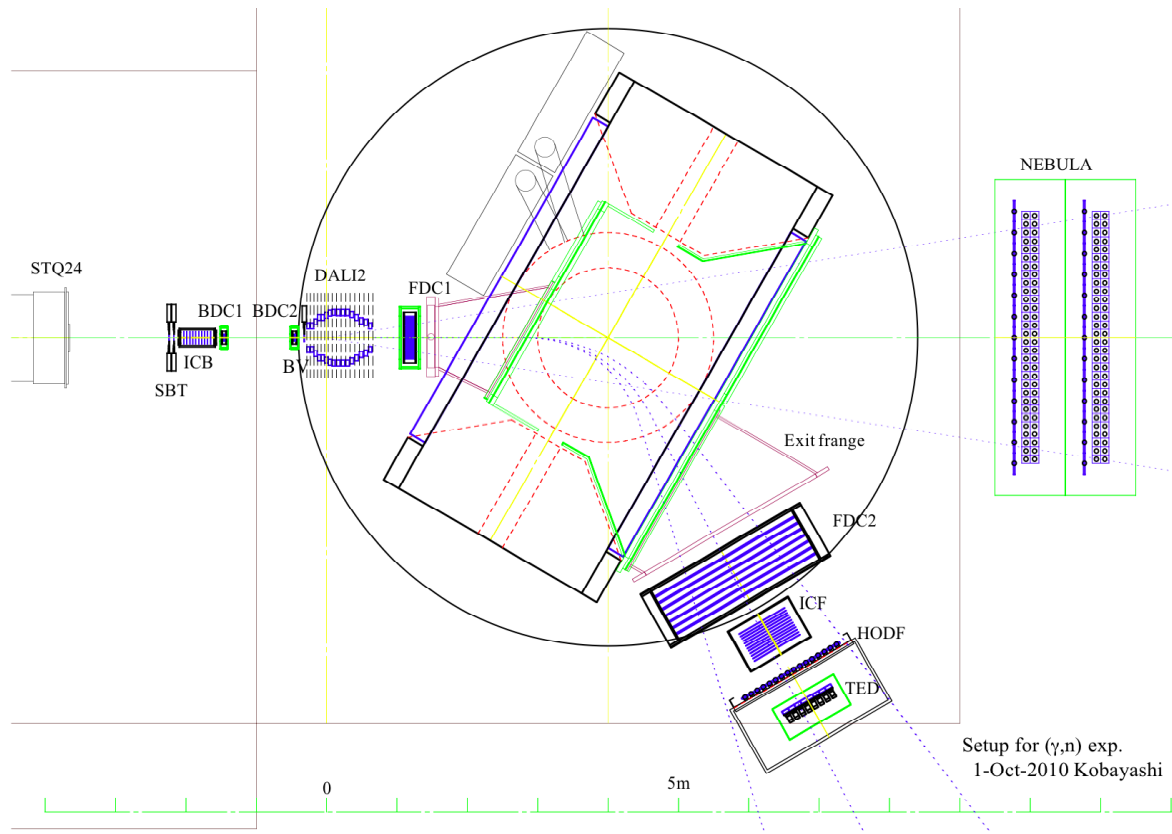
Fig. 2-10-1: Experimental setup in early 2012

Secondary beams are momentum tagged at F5 by BPC's. Two trigger scintillators, SBT's, are used as a start detector for trigger and also for measuring the charge of the incident beam. ICB is used to measure the charge for heavier beams. A gamma detector array, DALI2, is used to measure γ-rays emitted from the excited fragments produced in the decay process of Coulomb excitation. Use of DALI2 will be based on the collaboration with the Gamma group in RIKEN. FDC1 is used to measure the emission angle of the projectile fragments after combining the information of beam tracks. FDC2 and FDC1 are used for rigidity reconstruction. ICF is used to measure the charge of heavier fragments. HODF is used to measure the TOF and charge of the fragment. TED is used for measure the total energy of the heavy fragment. Particle identification of light fragments is performed by combining the information of charge and TOF measured by HODF and rigidity measured by FDC1 and FDC2. Particle identification of heavier fragments is performed by combining information of charges measured by ICF and HODF, TOF measured by HODF, total energy measured by TED, and rigidity measured by FDC1 and FDC2. Projectile-rapidity neutrons are detected by NEBULA.

A reaction target is placed 4 m downstream of the magnet center. NUBULA is set at 10 m from the reaction target, covering ±10 degrees in the horizontal direction and ±5 degrees in the vertical direction.